

### **Comments to the Author:**

The focus of this paper is an exploration of surface ozone levels predicted over India and adjacent regions using the WRF-Chem model, with two different chemical mechanisms, and three different emission inventories. The resulting predicted ozone fields are compared to each other, and to observations. The manuscript has received two detailed reviews, which raise a number of issues, the majority of which the authors have addressed, although with some areas where further refinement would improve the quality of the manuscript, and noted below.

**Response:** We thank the editor for thoroughly reviewing our work and for his valuable suggestions. The points raised (normal text) are addressed here (bold text). The corresponding changes made in the manuscript are highlighted in blue colour for added text and in red colour (strike out) for removed text. We are obviously open for any further comments and improvements in the manuscript, if needed.

**Comment:** The more substantive comment relates to the overall focus of the work. In particular, the referees challenge the use of emission inventories from very different years (2006, 2010, 2012), in a simulation for 2013, and which is compared with observational data acquired mostly between 2009 and 2013, but in some cases dating back to 2004 or earlier. The concern arises as there are substantial and well documented trends in ozone precursor emissions, and ozone levels, over this region. There are secondary concerns over the focus upon just O<sub>3</sub> rather than NO<sub>x</sub> and VOC as the model metrics (although addressed to an extent in the revised version), and station specific dependencies in some locations which regional model resolution cannot address.

**Response:** The old observations pointed out by the editor (2004 and before) has been removed in the revised version. We do realize that regional models cannot resolve the station specific dependencies of some locations. Still it should be noted that we have conducted simulations at higher resolution (12 km) than those in previous evaluation studies over South Asia (for example - 45 km by 45 km in Kumar et al., 2012b; 30 km by 30 km in Ojha et al., 2016). Also many of the stations used in the study are somewhat away from the roadside and generally inside the campus of universities/ institutes (see references provided in the Table 4) and therefore representing homogeneous conditions.

To make better model predictions at further higher resolution (than 12 km), development of finer resolution inventories than the ones used in the current study is also required over the region (HTAP and SEAC4RS are at 0.1 by 0.1 deg resolution which is around 11 km by 11 km). So we also recommend preparing high-resolution regional inventories for the anthropogenic emissions of O<sub>3</sub> precursors over South Asia, also accounting for year-to-year changes. This is also briefly discussed in the revised version (Page: 15, Lines: 583-586).

The results in the amended manuscript (i.e. most figures, tables) focus upon the difference in modelled ozone and ozone tendencies between the different inventories and chemical mechanisms, and exploration of the factors underpinning these. This is the appropriate focus for the manuscript, as the results cannot be readily compared with absolute ozone levels using

ozone observations 15 years adrift from the inventory, and different meteorological years etc. However the paper text still focuses substantially upon the comparisons with measurements – this focus should be adjusted, to comparison between inventories and chemical mechanisms, in a revised manuscript. The authors response to this point raised by the external referees – that better data do not exist – may be correct, but should lead to the conclusion that the comparison cannot therefore usefully be performed (at least, without explicit consideration of precursor and ozone observational trends, local station factors, and NO<sub>x</sub> and VOC measurements).

**Thanks for the suggestions. The paper text focusing upon the comparisons with measurements have been revised by comparing the patterns in different chemical environments (Page: 9, Lines: 328-335; Page: 12, Lines: 438-439; New Supplementary Figs. S6, and S12), as discussed in the response to Referee 1, comment 1, below. Focus has been on inter-comparison of model results more now. A simulation of differing year (2010), in addition to 2013, is kept in the manuscript to show the variability that it can induce in the simulated ozone and to show that the main conclusions of the paper are not affected if we simulate for a different meteorological year.**

Referee 1 comments

**Comment 1:** Focus should be upon ozone production between models, not absolute ozone levels. The (many) uncertainties in model chemistries need to be outlined in the paper, both between the two mechanism used, and overall

**Response 1:** Thanks for the suggestion and we have revised the manuscript in this direction. We include new figures (see revised supplement material; Fig. S6 and S12) to compare the ozone build up using  $\Delta O_3$ , which is the difference between diurnal mean and hourly values, for model simulations and observation at all stations. Thus the figure is useful in comparison between different simulations and observations without actually considering absolute ozone levels. The corresponding text is included in the revised manuscript (Page: 9, Lines: 328-335; Page: 12, Lines: 438-439).

The uncertainties relating to the chemical mechanisms have been added to the revised manuscript (Pages: 9-10, Lines: 355-361) as follows:

“Choice of chemical mechanisms in the regional models can also be an important element in the prediction of ozone. Inclusion of additional chemical species along with insufficient information on region-specific speciation factors could induce uncertainties to the predicted ozone. Further, in order to reduce the computational costs most chemical mechanisms in the models make use of lumping approach to reduce the number of chemical reactions thus avoiding treatment of all chemical species (Zaveri et al., 1999; Sarkar et al., 2016). In addition, different reaction rate constants, photolysis and dry deposition schemes used in the mechanisms are some of the factors leading to the uncertainties”.

The differences between the chemical mechanisms used in the study also have been mentioned in the revised manuscript (Page: 4, Lines: 150-154; Page: 10, Lines: 366-370) as follows:

**“In the present study, the photolysis rates are calculated using the Fast-J photolysis scheme (Wild et al., 2000) in RADM2 simulations and the Madronich FTUV scheme in the MOZART simulation. In WRF-Chem, the Madronich F-TUV photolysis scheme uses climatological O<sub>3</sub> and O<sub>2</sub> overhead columns. The treatment of dry deposition process also differs between RADM2 and MOZART owing to differences in Henry’s Law coefficients and diffusion coefficients.”**

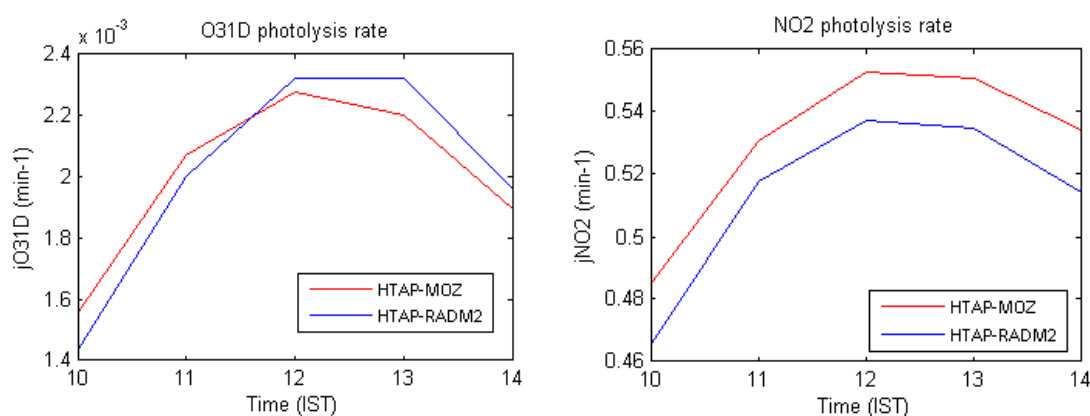
**Comment 3:** the comparison with observations is of limited use to guide the choice of “correct” answer given the issues outlined above – better comparison would be with newer emissions data. Local surface site factors (e. g. roadside etc) will dominate the NO<sub>x</sub> levels and hence O<sub>3</sub> levels – which cannot be captured in a regional model. Observations of “NO<sub>x</sub>” are probably (mostly) NO<sub>y</sub>, if heated Mo converter instruments are used for NO<sub>2</sub> detection.

**Response 3:** We agree and now explicitly mention these limitations in the revised version (Page: 13, Lines 490-493; Page: 15, Lines: 566-568). Many of the stations used in the study are somewhat away from the roadside and generally inside the campus of universities/ institutes (see references provided in the Table 4).

We agree that employing more sensitive techniques (e. g. blue light converter for NO<sub>2</sub>) in future would provide better insights into model performance in reproducing NO<sub>x</sub> over India. This is also mentioned in the revised version (Page: 7, Lines: 242-243).

**Comment 5:** please include an example of actual j values from the two photolysis schemes to allow the reader to understand the impact – e.g. a simple comparison of jNO<sub>2</sub> and jO(1D) for a surface point in the centre of the domain at midday

**Response 5:** Variation of required photolysis rates from 1000 IST to 1400 IST and their specific values at surface point in the centre of the domain (just for midday) is provided below for 15<sup>th</sup> April 2013. This is also now added in the revised manuscript (Page: 14, Lines: 534-535; Fig. S13 in supplement).



Chemical mechanism	Midday O1D photolysis rate (min-1)	Midday NO2 photolysis rate (min-1)
RADM2	0.0023	0.5375
MOZART	0.0023	0.5528

**Comment 11:** it would be useful to include the explanation for HCHO/NO<sub>y</sub> ratio in this manuscript. The work of Sillman et al refers primarily to a US context where VOC emissions (and hence VOC oxidation yields, ie HCHO formation) may be quite different to India – and referred to a specific trajectory duration / timepoint post emission - so the transition from NO<sub>x</sub> to VOC limitation may not occur at 0.28 in India, and will vary with post-emission processing duration.

**Response 11:** Sillman (1995) evaluated the correlation between O<sub>3</sub>-NO<sub>x</sub>-VOC sensitivity predicted by photochemical model and CH<sub>2</sub>O/NO<sub>y</sub> ratio. The correlation has been derived combining results from serial computations with the model by varying the anthropogenic and biogenic emissions, and meteorology. The method has been successfully employed in investigating ozone distribution over the South Asia (Kumar et al., 2012b), East Asia (Geng et al., 2007; Tie et al., 2013), and Europe (Mar et al., 2016). Tie et al (2013) reported similarities between the results based on the CH<sub>2</sub>O/NO<sub>y</sub> ratio and those following another method described by Kleinmann et al. (2003) over Shanghai.

The explanation has also been added to the revised manuscript (Page: 8, Lines: 287-293).

Additionally, the method has been used here to differentiate the ozone sensitivity between inventories so a shift in transitional value of 0.28 would not change the broad conclusions that differences exist in ozone sensitivity to precursors among model simulations.

**Comment 13:** The decision to turn off the aerosol radiation feedback is appropriate for the focus upon comparison between inventories (but not for comparison with absolute observed O<sub>3</sub> levels), this should be more clearly brought out / explained in the manuscript

**Response 13:** The suggested limitations are now clearly mentioned in the revised manuscript (Page: 13, Lines 490-493; Page: 15, Lines: 566-568). Comparison with absolute observed O<sub>3</sub> levels also has been substantially reduced.

**Comment 14:** Give specific values for the modelled vs observed water vapour data (ie comparison of means at surface / through profile, sonde profiles used etc).

**Response 14:** Meteorology is nudged towards Era-interim reanalysis thus limiting errors in simulations. Additionally, meteorological inputs and setup are similar among different simulations and therefore would not lead to significant differences in simulated chemistry.

Specific values are being provided below at lowest level of sonde observations available.

Station	Pressure level (hpa)	Modeled water vapour (g/kg)	Observed water vapour (g/kg)
Delhi	925	6.5±1.9	6.7±1.6
Bhubaneswar	1000	18.7±1.4	18.4±3.5
Ahmedabad	1000	9.7±3.0	11.1±2.2

Referee 2 comments

**Comment 1:** please advance explanations for the difference in model performance (between models, not vs observations) as this is the focus of the study and paper title

**Response 1:** Manuscript has been revised to focus more on the inter-comparison of model results. As mentioned to the response to referee 1 (comment 1), we have added new figures (see revised supplement material; Fig. S6 and S12) to compare the variability / patterns using  $\Delta O_3$  (mean  $O_3$ -hourly  $O_3$ ) between model and observations, which somewhat minimizes the effect of absolute ozone levels on comparison. The corresponding text is also suitably revised (Page: 9, Lines: 328-335; Page: 12, Lines: 438-439).

The old station data (pre 2004) have been completely removed and the comparison with observation in the revised manuscript is mostly based on diurnal variability rather than absolute numbers. The comparison of model results with observation (revised by excluding 2004 and old observation) averaged for all sites in the manuscript is however retained as to indicate (roughly) how average ozone values compare between model and recent observations (2009-2013), with a clear mention of the limitations associated with such a comparison (Page: 13, Lines 490-493; Page: 15, Lines: 566-568).

**Comment 2:** please expand on the impact of biomass burning effects in this work [not from literature] – ie from that aspect of the different emission inventories?

**Response 2:** The anthropogenic emission inventories used in the study exclude biomass burning emissions. So we have used biomass burning emissions from Fire Inventory from NCAR (FINN) that has been kept same in all simulations (Page: 5, Lines: 185-186). FINN emissions have been used in numerous modelling studies (e.g. Kumar et al., 2012b, Amnuaylojaroen et al., 2014). As the focus of this paper is only on reporting the differences between anthropogenic emission inventories in predicting ozone, the analysis of impact of biomass burning has not been conducted. Authors are collecting observations of fire tracers using a mass spectrometer and would follow up on the suggestion in a separate study.

**Comment 8:** the pre 2004 data may not be appropriate to use for the reasons noted above. If they are to be retained explicit consideration of the trends in  $O_3$  is needed – however the manuscript focus should compare the models.

**Response 8:** Pre-2004 data is completely removed in the revised version of the manuscript in all figures (see e.g. revised Table 4, Fig. 1, Fig. 6, Fig. 11 etc).

**Abstract** – needs to mention the second chemical mechanism, ie MOZART. Discussion of absolute model performance should be reduced given issues noted above.

**Response:** Name of mechanism is now mentioned (Page: 1, Line: 30). Discussion of absolute model performance is also reduced with more discussions on variability/ diurnal patterns and ozone build up using  $\Delta O_3$  now (Page: 9, Lines: 328-335; Page: 12, Lines: 438-439; New Supplementary Figs. S6 and S12).

## References

- Amnuaylojaroen, T., Barth, M. C., Emmons, L. K., Carmichael, G. R., Kreasuwun, J., Prasitwattanaseree, S., and 612 Chantara, S.: Effect of different emission inventories on modeled ozone and carbon monoxide in Southeast Asia, 613 *Atmos. Chem. Phys.*, 14, 12983-13012, doi:10.5194/acp-14-12983-2014, 2014.
- Geng, F., Zhao, C., Tang, X., Lu, G., and Tie, X.: Analysis of ozone and VOCs measured in Shanghai: A case study, *Atmos. Environ.*, 41, 989–1001, 2007.
- Kumar, R., Naja, M., Pfister, G. G., Barth, M. C., Wiedinmyer, C., and Brasseur, G. P.: Simulations over South 733 Asia using the Weather Research and Forecasting model with Chemistry (WRF-Chem): chemistry evaluation and 734 initial results, *Geoscientific Model Development* 5, 619-648, 2012b.
- Mar, K. A., Ojha, N., Pozzer, A., and Butler, T. M.: Ozone air quality simulations with WRF-Chem (v3.5.1) over Europe: model evaluation and chemical mechanism comparison, *Geosci. Model Dev.*, 9, 3699-3728, doi:10.5194/gmd-9-3699-2016, 2016.
- Ojha, N., Pozzer, A., Rauthe-Schöch, A., Baker, A. K., Yoon, J., Brenninkmeijer, C. A. M., and Lelieveld, J.: Ozone and carbon monoxide over India during the summer monsoon: regional emissions and transport, *Atmos. Chem. Phys.*, 16, 3013-3032, doi:10.5194/acp-16-3013-2016, 2016.
- Sarkar, M., Venkataraman, C., Guttikunda, S., and Sadavarte, P.: Indian emissions of technology-linked NMVOCs with chemical speciation: An evaluation of the SAPRC99 mechanism with WRF-CAMx simulations, *Atmospheric Environment*, 134, 70-83, <http://dx.doi.org/10.1016/j.atmosenv.2016.03.037>, 2016.
- Sillman, S.: The use of NO<sub>y</sub>, H<sub>2</sub>O<sub>2</sub> and HNO<sub>3</sub> as indicators for ozone-NO<sub>x</sub>-hydrocarbon sensitivity in urban locations, *J. Geophys. Res.*, 100, 14175–14188, 1995.
- Tie, X., Geng, F., Guenther, A., Cao, J., Greenberg, J., Zhang, R., Apel, E., Li, G., Weinheimer, A., Chen, J., and Cai, C.: Megacity impacts on regional ozone formation: observations and WRF-Chem modeling for the MIRAGE-Shanghai field campaign, *Atmos. Chem. Phys.*, 13, 5655-5669, <https://doi.org/10.5194/acp-13-5655-2013>, 2013.
- Wild, O., Zhu, X. and Prather, M. J.: Fast-J: Accurate simulation of in- and below cloud photolysis in tropospheric 853 chemical models, *Journal of Atmospheric Chemistry*, 37, 245-282, 2000.
- Zaveri, R. A. and Peters, L. K.: A new lumped structure photochemical mechanism for large-scale applications, *JOURNAL OF GEOPHYSICAL RESEARCH*, VOL. 104, NO. D23, PAGES 30387-30415, 1999.

# WRF-Chem simulated surface ozone over South Asia during the pre-monsoon: Effects of emission inventories and chemical mechanisms

Amit Sharma<sup>1, 2, \*</sup>, Narendra Ojha<sup>2, \*</sup>, Andrea Pozzer<sup>2</sup>, Kathleen A. Mar<sup>3</sup>, Gufran Beig<sup>4</sup>, Jos Lelieveld<sup>2, 5</sup>, and Sachin S. Gunthe<sup>1</sup>

<sup>1</sup>Department of Civil Engineering, Indian Institute of Technology Madras, Chennai, India

<sup>2</sup>Atmospheric Chemistry Department, Max Planck Institute for Chemistry, Mainz, Germany

<sup>3</sup>Institute for Advanced Sustainability Studies, Potsdam, Germany

<sup>4</sup>Indian Institute for Tropical Meteorology, Pune, India

<sup>5</sup>Energy, Environment and Water Research Center, The Cyprus Institute, Nicosia, Cyprus

\*Correspondence to: Amit Sharma ([amit.iit87@gmail.com](mailto:amit.iit87@gmail.com)) and Narendra Ojha ([narendra.ojha@mpic.de](mailto:narendra.ojha@mpic.de))

## Abstract

We evaluate numerical simulations of surface ozone mixing ratios over the South Asian region during the pre-monsoon season, employing three different emission inventories (EDGAR-HTAP, INTEX-B, and SEAC4RS) in the WRF-Chem model with the RADM2 chemical mechanism. Evaluation of diurnal variability in modelled ozone and its diurnal variability, using as compared to observational data from a network of 18 15 monitoring stations across South Asia shows the model ability to reproduce the clean, rural and polluted urban conditions over this region. In contrast to the diurnal average, the modelled ozone mixing ratios during noontime i.e. hours of intense photochemistry (1130-1630 h Indian Standard Time or IST) are found to differ among the three inventories. This suggests that evaluations of the modelled ozone limited to 24-h average are insufficient to assess uncertainties associated with ozone build-up. HTAP generally shows 10-30 ppbv higher noontime ozone mixing ratios than SEAC4RS and INTEX-B, especially over the north-west Indo-Gangetic Plain (IGP), central India and southern India. Further, the model performance shows strong spatial heterogeneity, with SEAC4RS leading to better agreement with observations over east and south India, whereas HTAP performs better over north and central India, and INTEX-B over west India. The Normalized Mean Bias (NMB in %) in the noontime ozone over the entire South Asia is found to be lowest for the SEAC4RS (~9.7%), followed by INTEX-B (~11.5%) and HTAP (~20.9%). The HTAP simulation repeated with the alternative MOZART chemical mechanism showed even more strongly enhanced surface ozone mixing ratios (noontime NMB=34.2%) due to vertical mixing of enhanced ozone that has been produced aloft. The SEAC4RS inventory with the RADM2 chemical mechanism is found to be the most successful overall among the configurations evaluated here in simulating ozone air quality over South Asia. Our study indicates the need to also evaluate the O<sub>3</sub> precursors across a network of stations and the development of high-resolution regional inventories for the anthropogenic emissions over South Asia accounting for year-to-year changes to further reduce uncertainties in modelled ozone over this region. We also recommend preparing high-resolution regional inventories for the anthropogenic emissions of O<sub>3</sub> precursors over South Asia that also account for year-to-year changes.

## 1. Introduction

Tropospheric ozone plays central roles in atmospheric chemistry, air quality and climate change. Unlike primary pollutants, which are emitted directly, tropospheric ozone forms photochemically involving precursors such as carbon monoxide (CO), volatile organic compounds (VOCs) and oxides of nitrogen (NO<sub>x</sub>), supplemented by transport from the stratosphere (e.g. Crutzen, 1974; Atkinson, 2000; Monks et al., 2015). It can be transported over long distances resulting in enhanced concentrations even in areas located remote from the sources of precursors (Cox et al., 1975). The photochemical production of ozone and its impacts on agricultural crops and human health are especially pronounced near the surface. Numerous studies have shown that elevated surface ozone levels significantly reduce crop yields (e. g.; Krupa et al., 1998; Emberson et al., 2009; Ainsworth et al., 2012; Wilkinson et al., 2012), in addition to adverse human health effects that cause premature mortality (e.g., Bell et al., 2004; Jerrett et al., 2009; Anenberg et. al., 2010; Lelieveld et al., 2015).

An accurate representation of anthropogenic emissions of ozone precursors is essential to understand the photochemical production of ozone and support policy making. While anthropogenic emissions have been nearly stable or decreasing over northern America and Europe (e. g. Yoon and Pozzer, 2014), there has been substantial enhancement over the East and South Asian regions in recent decades (e. g. Akimoto, 2003; Ohara et al., 2007, Logan et al., 2012; Gurjar et al., 2016). The number of premature mortalities per year due to outdoor air pollution is anticipated to double by the year 2050 as compared to the year 2010 in a business-as-usual scenario, predominantly in Asia (Lelieveld et al., 2015). The multi-pollutant index over all populated regions in the northern hemisphere shows a general increase, with South Asia being the major hotspot of deteriorating air quality (Pozzer et al., 2012).

The growth of anthropogenic emissions over the South Asian region has regional implications, and is also predicted to influence air quality on a hemispheric scale (Lelieveld and Dentener, 2000). It was shown that the anthropogenic emissions and their subsequent photochemical degradation over South Asia influence air quality over the Himalayas (e.g. Ojha et al., 2012; Sarangi et al., 2014) and the Tibetan Plateau (Lüthi et al., 2015) as well as the marine environment downwind of India (e.g. Lawrence and Lelieveld, 2010). Additionally, the prevailing synoptic scale weather patterns make this region highly conducive to long-range export of pollutants (e.g. Lelieveld et al., 2002; Lawrence et al., 2003; Ojha et al., 2014; Zanis et al., 2014). Therefore, the accurate estimation of anthropogenic emissions over South Asia and their representation in chemical transport models are essential to quantify the effects on regional as well as global air quality.

The Weather Research and Forecasting model with Chemistry (WRF-Chem) (Grell et al., 2005; Fast et al., 2006), a regional simulation system, has been popular for use over the South Asian region in numerous recent studies to simulate the meteorology and spatio-temporal distribution of ozone and related trace gases (e. g. Kumar et al., 2012a, 2012b; Michael et al., 2013; Gupta et al., 2015; Jena et al., 2015; Ansari et al., 2016; Ojha et al., 2016; Girach et al., 2017). WRF-Chem simulations at higher spatial resolution employing regional emission inventories have been shown to better reproduce the observed spatial and temporal heterogeneities in ozone over this region as compared to the global models (e.g. Kumar et al., 2012b; Ojha et al., 2016). However, an evaluation of modelled ozone based on data from a network of stations across South Asia is imperative considering very large spatio-temporal heterogeneity in the distribution of ozone over this region (e.g. Kumar et al., 2010; Ojha et al., 2012; Kumar et al., 2012b) mainly resulting from heterogeneous precursor sources and population distribution. WRF-



Chem simulated ozone distributions have also been utilized to assess the losses in crop yields, and it was suggested that the estimated crop losses would be sufficient to feed about 94 million people living below the poverty line in this region (Ghude et al., 2014). Further, WRF-Chem has been used to estimate that premature mortality in India caused by chronic obstructive pulmonary disease (COPD) due to surface O<sub>3</sub> exposure was ~12,000 people in the year 2011 (Ghude et al., 2016). Despite these applications, there is room for improvement in modeled concentrations as some limited studies evaluating ozone on diurnal scales revealed a significant overestimation of noontime ozone e.g. by as much as 20 ppbv in Kanpur (Michael et al., 2013) and 30 ppbv in Delhi (Gupta and Mohan, 2015).

Using WRF-Chem, Amnuaylojaroen et al. (2014) showed that over continental southeast Asia surface ozone mixing ratios vary little (~4.5%) among simulations employing different emission inventories. A recent study by Mar et al. (2016) highlighted the dependence of WRF-Chem predicted ozone air quality (over Europe) on the chosen chemical mechanism. These results indicate the need for evaluating the effects of emission inventories and chemical mechanisms on the model performance using a network of stations across South Asia, which has not been carried out thus far. The main objectives of the present study are:

- (a) To evaluate WRF-Chem simulated ozone over South Asia, especially the ~~including the~~ diurnal cycle variability, against recent in situ measurements from ~~a network of~~ stations representing different chemical environments (urban, rural, clean etc.);
- (b) To inter-compare model simulated O<sub>3</sub> among different emission inventories;
- (c) To inter-compare model simulated O<sub>3</sub> between two extensively used chemical mechanisms (MOZART and RADM2) with the same emission inventory;
- ~~(d) To provide recommendations on the model configuration for future studies over stations, sub-regions as well as the entire South Asian region.~~

We focus on the pre-monsoon season (March-May) for the study as O<sub>3</sub> mixing ratios at the surface are generally the highest over most of South Asia during this period (Jain et al., 2005; Debaje et al., 2006; Reddy et al., 2010; Ojha et al., 2012; Gaur et al., 2014; Renuka et al., 2014; Bhuyan et al., 2014; Sarangi et al., 2014; Yadav et al., 2014; Sarkar et al., 2015). This is because photochemistry over South Asia is most intense during this season caused by the combined effects of high pollution loading, biomass-burning emissions and a lack of precipitation. The effects of biomass burning on ozone in Southern Asia have been studied by Jena et al. (2014) reporting O<sub>3</sub> enhancements of 4-10 ppb (25-50%) in the Eastern region including Burma, 1-3 ppb (10-25%) in Central India and 1-7 ppb (4-10%) in the Indo-Gangetic region. Further, the O<sub>3</sub> enhancement was found to be about 2-6 ppb (8-20%) over the Bay of Bengal in March, which was attributed to transport from the Eastern region. Section 2 presents the model description, including physics and chemistry options, emission inputs and the observational data. Model evaluation focussing on the effects of different emission inventories on ozone is presented in section 3. The inter-comparison between the RADM2 and MOZART chemical mechanism is discussed in section 4. The sub-regional and South Asian domain evaluation and recommendations on model configuration are provided in section 5, followed by the summary and conclusions drawn from the study in section 6. The list of abbreviations and acronyms used in this paper are listed in Table 1.

## 2. Methodology

### 2.1. WRF-Chem

In this study we use the Weather Research and Forecasting model coupled with chemistry (WRF-Chem version 3.5.1), which is an online mesoscale model capable of simulating meteorological and chemical processes simultaneously (Grell et al., 2005; Fast et al., 2006). The model domain (Fig. 1) is defined on a mercator projection and is centred at 22° N, 83° E with 274 and 352 grid points in the east-west and north-south directions, respectively, at the horizontal resolution of 12 km x 12 km. The land use data is incorporated from the US Geological Survey (USGS) based on 24 land use categories. The ERA-interim reanalysis dataset from ECMWF (<http://www.ecmwf.int/en/research/climate-reanalysis/browse-reanalysis-datasets>), archived at the horizontal resolution of about 0.7° and temporal resolution of 6 hours, is used to provide the initial and lateral boundary conditions for the meteorological calculations. All simulations in the study have been conducted for the period: 26<sup>th</sup> February – 31<sup>st</sup> May, 2013 at a time step of 72 s. The model output is stored every hour for analysis. The first three days of model output have been discarded as model spin up.

Radiative transfer in the model has been represented using the Rapid Radiative Transfer Model (RRTM) longwave scheme (Mlawer, 1997) and the Goddard shortwave scheme (Chou and Suarez, 1994). Surface physics is parameterized using the Unified Noah land surface model (Tewari et al., 2004) along with eta similarity option (Monin and Obukhov, 1954; Janjic, 1994, 1996), and the planetary boundary layer (PBL) is based on the Mellor-Yamada-Janjic (MYJ) scheme (Mellor and Yamada, 1982; Janjic, 2002). The cloud microphysics is represented by the Lin et al. scheme (Lin et. al., 1983), and cumulus convection is parameterized using the Grell 3D Ensemble Scheme (Grell, 1993; Grell and Devenyi, 2002). Four-dimensional data assimilation (FDDA) is incorporated for nudging to limit the drift in the model simulated meteorology from the ERA-interim reanalysis (Stauffer and Seaman, 1990; Liu et al. 2008). Horizontal winds are nudged at all vertical levels, whereas temperature and water vapour mixing ratios are nudged above the PBL (Stauffer et al. 1990, 1991). The nudging coefficients for temperature and horizontal winds are set as  $3 \times 10^{-4} \text{ s}^{-1}$  whereas it is set as  $10^{-5} \text{ s}^{-1}$  for water vapour mixing ratio (Otte, 2008).

This study utilizes two different chemical mechanisms, the Regional Acid Deposition Model - 2<sup>nd</sup> generation (RADM2) (Stockwell et al., 1990), and the Model for Ozone and Related Chemical Tracers-version 4 (MOZART-4) (Emmons et al., 2010). RADM2 chemistry includes 63 chemical species participating in 136 gas phase and 21 photolysis reactions. MOZART chemistry includes 81 chemical species participating in 159 gas phase and 38 photolysis reactions. Aerosols are represented using the Modal Aerosol Dynamics Model for Europe/ Secondary Organic Aerosol Model (MADE/-SORGAM) (Ackermann et al., 1998; Schell et al., 2001) with RADM2 and Global Ozone Chemistry Aerosol Radiation and Transport (GOCART) (Chin et al., 2000) with MOZART. The photolysis rates are calculated using the Fast-J photolysis scheme (Wild et al., 2000) in RADM2 simulations and the Madronich FTUV scheme in the MOZART simulation. In WRF-Chem, the Madronich F-TUV photolysis scheme uses climatological O<sub>3</sub> and O<sub>2</sub> overhead columns. The treatment of dry deposition process also differs between RADM2 and MOZART owing to differences in Henry's Law coefficients and diffusion coefficients. The chemical initial and lateral boundary conditions are provided from 6 hourly fields from the Model for Ozone and Related Chemical Tracers (MOZART-4/GEOS5) (<http://www.acom.ucar.edu/wrf-chem/mozart.shtml>).

## 2.2. Emission inputs

This study utilizes three different inventories for the anthropogenic emissions: HTAP, INTEX-B and the SEAC4RS, which are briefly described here. The Hemispheric Transport of Air Pollution (HTAP) inventory (Janssens-Maenhout et al., 2015) for anthropogenic emissions ([http://edgar.jrc.ec.europa.eu/htap\\_v2/index.php?SECURE=\\_123](http://edgar.jrc.ec.europa.eu/htap_v2/index.php?SECURE=_123)) available for the year 2010 has been used. The HTAP inventory has been developed by complementing various regional emissions with EDGAR data, in which Asian region including India is represented by the Model Intercomparison study for Asia (MICS-Asia) inventory, which is at a horizontal resolution of  $0.25^{\circ} \times 0.25^{\circ}$  (Carmichael et al., 2008). The resultant global inventory is re-gridded at the spatial resolution of  $0.1^{\circ} \times 0.1^{\circ}$  and temporal resolution of 1 month. HTAP includes emissions of CO, NO<sub>x</sub>, SO<sub>2</sub>, NM VOCs, PM, BC and OC from power, industry, residential, agriculture, ground transport and shipping sectors. The Intercontinental Chemical Transport Experiment-Phase B (INTEX-B) inventory (Zhang et al., 2009), developed to support the INTEX-B field campaign by the National Aeronautics and Space Administration (NASA) in spring 2006, is the second inventory used in this study. It provides total emissions for year 2006 at a horizontal resolution of  $0.5^{\circ} \times 0.5^{\circ}$ . The emission sectors include power generation, industry, residential and transportation. The Southeast Asia Composition, Cloud, Climate Coupling Regional Study (SEAC4RS) inventory (Lu and Streets, 2012), prepared for the NASA SEAC4RS field campaign, is the third inventory used in this study. It provides total emissions for the year 2012 at a spatial resolution of  $0.1^{\circ} \times 0.1^{\circ}$ . The SEAC4RS and INTEX-B did not cover regions in the north western part of the domain, and therefore we complemented this region (longitude <  $75^{\circ}$  E and latitude >  $25^{\circ}$  N) by HTAP emission data. The emissions of CO, NM VOCs and NO<sub>x</sub> emissions among the three emission inventories, as included in the simulations, are shown in Fig. 2. Table 2 provides estimates of total emissions over different regions (as defined in Fig.1) from the three inventories. The total emissions over all regions show that HTAP has about 43% higher and SEAC4RS about 46% higher NO<sub>x</sub> emissions compared to the INTEX-B inventory. Also, HTAP has about 37% higher VOC emissions compared to SEAC4RS and about 49% higher compared to the INTEX-B inventory. Hence SEAC4RS, the most recent inventory of the three, has similar total NO<sub>x</sub> emissions as that in HTAP but the total VOC source is closer to INTEX-B, which is the oldest of the three inventories. Considering the non-linear dependence of O<sub>3</sub> formation on precursors, numerical experiments are necessary to assess the influence of such large differences among the inventories. The emissions from biomass burning are included using the Fire Inventory from NCAR (FINN) version 1.0 (Wiedinmyer et al., 2011). Model of Emissions of Gases and Aerosols from Nature (MEGAN) is used to include the biogenic emissions (Guenther et al., 2006) in the model.

The HTAP inventory is available at monthly temporal resolution while INTEX-B and SEAC4RS are available as annual averages; however, seasonal variability in anthropogenic emissions may not have a major effect in this study as we focus here on spring (pre-monsoon), for which monthly emissions are similar to the annual mean (seasonal factor close to unity) (Supplementary material - Fig. S1; also see Fig. 2b in Kumar et al., 2012b). Nevertheless, seasonal influence during spring is strongest for biomass-burning emissions, which have been accounted for. The emissions from all inventories were injected in the lowest model layer. The diurnal profiles of the anthropogenic emissions of ozone precursors, specific to South Asia are not available. A sensitivity simulation implementing the diurnal emission profile available for Europe (Mar et al., 2016 and references therein) showed a little impact on predicted noontime ozone over South Asia (Supplementary material – Fig S2).

### 2.3. Simulations

We have conducted 4 different numerical simulations as summarized in Table 3 and briefly described here. Three simulations correspond to three different emission inventories HTAP, INTEX-B and SEAC4RS for the anthropogenic emissions of ozone precursors, employing the RADM2 chemical mechanism. These simulations are named HTAP-RADM2, INTEX-RADM2 and S4RS-RADM2 respectively. The emissions of aerosols have been kept same (HTAP) among these three simulations and aerosol-radiation feedback has been switched off to specifically identify the effects of emissions of O<sub>3</sub> precursors on modelled ozone. An additional simulation HTAP-MOZ has been conducted to investigate the sensitivity of ozone to the employed chemical mechanism (MOZART vs RADM2) by keeping the emissions fixed to HTAP.

### 2.4. Observational dataset

Previous studies have shown that WRF-Chem accurately reproduces the synoptic scale meteorology over the Indian region, justifying its use for atmospheric chemical simulations (e. g. Kumar et al., 2012a). Further, nudging towards reanalysis data limits deviations in simulated meteorology (e. g. Kumar et al., 2012a; Ojha et al., 2016; Girach et al., 2017). Nevertheless, we include an evaluation of model simulated water vapour, temperature and wind speed against radiosonde observations (Supplementary material, Fig. S3). Vertical profiles of the monthly average (April) water vapour mixing ratio (g/Kg), temperature (°C) and horizontal wind speed (m/s) have been obtained from radiosonde data (available at <http://weather.uwyo.edu/upperair/sounding.html>) for evaluation of modelled meteorology over Delhi (in North India), Bhubaneswar (in east India) and Ahmedabad (in west India). We find that model simulated meteorology is in good agreement (within 1-standard deviation variability) with the observations.

Surface ozone data is acquired from various studies and sources, as given in Table 4. In general, surface O<sub>3</sub> measurements over these stations have been conducted using the well-known technique of UV light absorption by ozone molecules at about 254 nm, making use of Beer-Lambert's Law. The accuracy of these measurements is reported to be about 5% (Kleinmann et al., 1994). The response time of such instruments is about 20 s and instruments have a lower detection limit of 1 ppbv (Ojha et al., 2012). Here we have used the hourly and monthly average data for the model evaluation. The details of instruments and calibrations at individual stations can be found in the references given in the Table 4. **It is to be noted that most of the observations are conducted generally inside the campus of universities/ institutes, reasonably away from the direct roadside emissions / exhausts (see references provided in Table 4) and therefore not influenced by concentrated local pollution sources.**

As simultaneous measurements at different stations are very sparse over South Asia, the model evaluation has often to be conducted using observations of the same season/month of a different year (e. g. Kumar et al., 2012b; Kumar et al., 2015; Ojha et al., 2016). However, to minimize the effect of temporal differences we preferentially used measurements of recent years i.e. the observations at ~~~83% of~~ the stations used in this study are of the period: 2009-2013. For four stations: Delhi (north India), Jabalpur (central India), Pune (west India) and Thumba (south India), the observations and simulations are for the same year (2013). ~~The observations at three stations have been collected in previous periods (2004 or before).~~ Finally, we investigated the effects of temporal differences on the results and model biases presented here by conducting another simulation for a different year (2010) (Supplementary material, Fig. S4).

There is also a need to evaluate precursor mixing ratios over the region to further reduce uncertainties in modelled ozone over South Asia. However, very limited data is available for ozone precursors in India and adjacent countries (especially for non-methane volatile organic compounds; NMVOCs). We include an evaluation of modelled NO<sub>x</sub>, ethane and ethene mixing ratios against several recent observations in the supplementary material (see Section S1 and Table S1 on Pages 1-2). [More sensitive techniques \(e.g. blue light converter for NO<sub>2</sub>\) in future would provide better insights into model performance in reproducing NO<sub>x</sub> over India.](#)

### 3. Effects of emission inventories

#### 3.1. Spatial distribution of Ozone

The spatial distribution of WRF-Chem simulated 24-h monthly average ozone during April is shown in Fig. 3a (upper panel) for the three different emission inventories (HTAP, INTEX, and SEAC4RS). Generally the months of March and May are marked with seasonal transition from winter to summer and summer to monsoon respectively. Hence, the month of April is chosen to represent the pre-monsoon season as it is not influenced by these seasonal transitions, and the observational data is available for a maximum number of stations during this month for the comparison. The 24-h average ozone mixing ratios are found to be 40-55 ppbv over most of the Indian subcontinent for all the three inventories. Model simulated ozone levels over the coastal regions are also similar (30-40 ppbv) among the three inventories. The highest ozone mixing ratios (55 ppbv and higher) predicted in the South Asian region are found over northern India and the Tibetan Plateau. The WRF-Chem simulated spatial distributions of average ozone shown here are in agreement with a previous evaluation study over South Asia (Kumar et al., 2012b). Further, it is found that qualitatively as well as quantitatively the HTAP, INTEX-B and SEAC4RS lead to very similar distributions of 24-h average ozone over most of the South Asian region. The 24h monthly average ozone from observations is superimposed on the model results in Fig. 3a for comparison. WRF-Chem simulated distributions of average O<sub>3</sub> are in general agreement with the observational data (Fig. 3a), except at a few stations near coasts (e. g. Kannur and Thumba) and in complex terrain (Pantnagar and Dibrugarh). In contrast to the distribution of 24-h average O<sub>3</sub>, the noontime (1130-1630 IST) O<sub>3</sub> mixing ratios over continental South Asia exhibit significant differences among the three emission inventories (Fig. 3b). HTAP clearly leads to higher noontime O<sub>3</sub> mixing ratios, the difference being up to 10 ppbv over the Indo-Gangetic plain (IGP), 20 ppbv over Central India, and 30 ppbv over Southern India, compared to INTEX-B and SEAC4RS. The mean bias (MB) (model-observation) for 24-h and noontime average ozone at individual stations is provided in the supplementary material - Table S2 and S3. A sensitivity simulation is conducted to reveal the influence of a different cumulus parameterization (Kain-Fritsch scheme) on our conclusions. The differences in the modelled surface ozone mixing ratios over most of the Indian domain are found to be within  $\pm 5\%$  (supplementary material; Figure S5). The relatively large differences over some of the Indian region indicate that the Kain-Fritsch scheme tends to predict higher surface ozone mixing ratios relative to the base run (incorporating Grell 3D Ensemble Scheme), which would only add up to biases in the original runs. Therefore our conclusions are not affected.

The net photochemical O<sub>3</sub> production rate (ppbv h<sup>-1</sup>) from sunrise to noontime (0630-1230 IST), when most of the photochemical build-up of ozone takes place leading to its peak noontime mixing ratio, has been calculated utilizing the chemical tendencies in WRF-Chem (Barth et al., 2012; Girach et al., 2017). A comparison of monthly average O<sub>3</sub> production rates among the three inventories is shown in Fig. 4. As seen also from the O<sub>3</sub> mixing ratios (Fig. 3b), the HTAP emissions result in faster O<sub>3</sub> production ( $\sim 9$  ppbv h<sup>-1</sup>) throughout the IGP region. The highest

O<sub>3</sub> production rates for INTEX-B and SEAC4RS inventories are simulated only in the East Indian regions including the eastern parts of the IGP. It is noted that the rate of O<sub>3</sub> production is lower (4-8 ppbv h<sup>-1</sup>) over most of the south-western IGP for the INTEX-B and SEAC4RS inventories. Differences are also found over the southern Indian region with stronger ozone production in HTAP, followed by INTEX-B and SEAC4RS.

Figure 5 provides insight into the spatial distribution of O<sub>3</sub> production regimes estimated through the CH<sub>2</sub>O/NO<sub>y</sub> ratio (Geng et al., 2007; Kumar et al. 2012b) calculated during 0630 – 1230 IST, to help explain the differences in modelled ozone mixing ratios among the three simulations. The metric CH<sub>2</sub>O/NO<sub>y</sub>, as described by Sillman (1995), is suggested to be a useful diagnostic to determine the ozone production regime. ~~than by simply analysing the NO<sub>x</sub> and NMHC loadings is found in Sillman (1995).~~ Sillman (1995) evaluated the correlation between O<sub>3</sub>-NO<sub>x</sub>-VOC sensitivity predicted by photochemical model and CH<sub>2</sub>O/NO<sub>y</sub> ratio. The correlation has been derived combining results from serial computations with the model by varying the anthropogenic and biogenic emissions, and meteorology. The method has been successfully employed in investigating ozone distribution over the South Asia (Kumar et al., 2012b), East Asia (Geng et al., 2007; Tie et al., 2013), and Europe (Mar et al., 2016). Tie et al (2013) reported similarities between the results based on the CH<sub>2</sub>O/NO<sub>y</sub> ratio and those following another method described by Kleinmann et al. (2003) over Shanghai. A value of 0.28 for CH<sub>2</sub>O/NO<sub>y</sub> ratio is suggested to be the transitional value from VOC limited regime to NO<sub>x</sub> limited regime. The spatial distribution of regimes in all simulations in the present study is largely consistent with the findings of Kumar et al. (2012b) although the latter performed the analysis for afternoon hours (1130 – 1430 IST). The S4RS-RADM2 simulation predicts the entire IGP to be VOC sensitive whereas in HTAP-RADM2 and INTEX-RADM2 simulations though the northwest IGP and eastern IGP are VOC sensitive, the central IGP is mostly NO<sub>x</sub> limited. The coastal regions are also predicted to be VOC limited in all the three simulations. With the north-western IGP being VOC limited in all simulations, the noontime ozone mixing ratios are found to be higher in this region in HTAP-RADM2 simulation because of high NMVOC emissions in HTAP inventory as evident from figure 2 and table 2. Similar differences are also apparent in southern India.

In summary, these results show similar 24-h average ozone distributions but large differences in the ozone build-up until noon. The net photochemical ozone production in the morning hours (0630-1230) is shown to be sensitive to the different inventories over this region, which is attributed to differences in total NO<sub>x</sub> and/or NMVOC emissions. We therefore suggest that a focus on 24-h averages only would be insufficient to evaluate the ozone budget and implications for human health and crop yield. Next we compare the modeled diurnal ozone variations from three inventories with in situ measurements over 15 stations across the South Asia.

### 3.2. Diurnal variation

A comparison of WRF-Chem simulated diurnal ozone variability with recent in situ measurements over a network of 15 stations in the South Asian region is shown in Fig. 6. WRF-Chem is found to successfully reproduce the characteristic diurnal ozone patterns observed over the urban (e.g. Mohali, Delhi, Kanpur, Ahmedabad, Bhubaneswar and Pune) and rural (e.g. ~~Joharapur, Anantpur, Gadanki~~) stations, indicating strong ozone build-up from sunrise to noontime and the predominance of chemical titration (by NO) and deposition losses during the night. In general, WRF-Chem captures the daily amplitude of O<sub>3</sub> changes at relatively cleaner and high altitude stations, typically showing less pronounced diurnal variability, such as Nainital in the Himalayas ~~and Mt. Abu in~~



the Aravalli mountain range, although with differences in timing when model and observations attain minimum ozone mixing ratios, thus leading to relatively low correlation coefficient (see later in the text). For example, modelled diurnal amplitudes at Nainital are estimated to be ~19.2 ppbv (HTAP-RADM2), ~17.5 ppbv (INTEX-RADM2) and ~17.9 ppbv (S4RS-RADM2) as compared to the observational value of ~15.1 ppbv. The model does not reproduce the ozone mixing ratios at Pantnagar and Jabalpur except for afternoon peak values. This can be attributed to the role of complex terrain (presence of the Himalayas near Pantnagar), which cannot be fully resolved, even at 12 km resolution. Jabalpur is also surrounded by forests, hills and mountains (Sarkar et al., 2015), and such variability in a small area could impact the accuracy of model predictions. The model typically overestimates the noontime ozone mixing ratios over several urban (e.g. Kanpur, Ahmedabad, Haldia, Thumba) and rural stations (e.g. Joharapur, Kannur), which is attributed to the uncertainties in the emissions. The diurnal variability in O<sub>3</sub> indicated by  $\Delta O_3$ , i.e. the difference between diurnal mean and hourly values, is further compared between the model and observations at all the stations (Supplementary material – Fig S6). This comparison intends to focus more on to evaluate the model's ability to reproduce different diurnal patterns over urban, rural and clean chemical environments and minimizing the representation of absolute ozone levels. It is seen that model successfully captures the observed variability in ozone at most of the sites in this region. However, a limitation is noticed in resolving well the stations in the vicinity of complex terrain (such as Jabalpur), attributed to the stronger spatial heterogeneity due to forests, hills and mountains within a small area (Sarkar et al., 2015).

To briefly evaluate the possible effects due to the difference in meteorological year between model and observations, we repeated the HTAP-RADM2 simulation for a different year (2010) as shown in the Supplementary material – Fig. S4. The effect of changing the meteorological year in the model simulation is generally small (mostly within  $\pm 3$  ppbv in 3 years), except at a few stations in the north (Nainital and Pantnagar) and east (Haldia and Bhubaneswar). The effect is seen to vary from 4.8 ppbv to 6 ppbv (in 3 years) at these four three stations. These differences are found to be associated with the inter-annual variations in the regional and transported biomass burning emissions, as seen from MODIS fire counts and MOZART/GEOS5 boundary conditions (not shown here).

The model ability to reproduce diurnal variations at all stations is summarised using a Taylor diagram (Taylor, 2001) in Figure 7. The statistics presented are normalised standard deviation (SD), normalised centred root mean squared difference (RMSD) and the correlation coefficient. The normalisation of both SD and RMSD is done using the standard deviation of the respective observational data. The point indicated as 'REF' represents the observational data against the model results evaluated. WRF-Chem simulations show reasonable agreement with observations showing correlation coefficients generally greater than 0.7 for most sites. The locations such as Nainital, Mt. Abu and Jabalpur for which r values are lower (0.3-0.7) are associated with unresolved complex terrain, as mentioned earlier. Note that the Taylor diagram has been used to present evaluation statistics for a general overview and inter-comparison i.e. how the model reproduces the diurnal variation at different stations, irrespective of the emission inventory.

#### 4. Effects of chemical mechanism (RADM2 vs MOZART)

Choice of chemical mechanisms in the regional models can also be an important element in the prediction of ozone. Inclusion of additional chemical species along with insufficient information on region-specific speciation factors could induce uncertainties to the predicted ozone. Further, in order to reduce the computational costs most

chemical mechanisms in the models make use of lumping approach to reduce the number of chemical reactions thus avoiding treatment of all chemical species (Zaveri et al., 1999; Sarkar et al., 2016). In addition, different reaction rate constants, photolysis and dry deposition schemes used in the mechanisms are some of the factors leading to the uncertainties. A recent WRF-Chem evaluation over Europe showed better agreement with in situ measurements when the MOZART chemical mechanism was employed, compared to RADM2 (Mar et al., 2016). Following up on this, here we compare modelled ozone mixing ratios obtained with these two extensively used chemical mechanisms over South Asia: RADM2 (e. g. Michael et al., 2013; Ojha et al., 2016, Girach et al., 2017) and MOZART (e. g. Ghude et al., 2014; Ghude et al., 2016), keeping the same input emission inventory (HTAP). In the present study, the photolysis rates are calculated using the Fast-J photolysis scheme (Wild et al., 2000) in RADM2 simulations and the Madronich FTUV scheme in the MOZART simulation. In WRF-Chem, the Madronich F-TUV photolysis scheme uses climatological  $O_3$  and  $O_2$  overhead columns. The treatment of dry deposition process also differs between RADM2 and MOZART owing to differences in Henry's Law coefficients and diffusion coefficients. Thus, the following sensitivity analysis is aimed at exploring if the use of the more detailed chemical mechanism of MOZART could improve the model performance.

#### 4.1. Spatial distribution of surface $O_3$

The WRF-Chem simulated spatial distributions of 24-h average and noontime average surface ozone are compared in Fig. 8. The monthly values of the 24-h and noontime ozone mixing ratios from measurements are also shown. Overall, the average ozone mixing ratios over South Asia are simulated to be higher with the MOZART chemical mechanism compared to RADM2, which is consistent with the results of Mar et al. (2016) for the European domain. The 24-h average ozone mixing ratios over India simulated with MOZART chemistry are found to be higher than those with RADM2 chemistry, especially over the eastern Indian region (~60 ppbv and more for MOZART compared to ~40-55 ppbv for RADM2). Average ozone levels over the coastal regions are found to be similar between the two mechanisms (30-40 ppbv). MOZART chemistry also predicts high 24-h average ozone mixing ratios (55 ppbv and higher) over the Tibetan Plateau region, similar to RADM2. A striking difference between the two chemical mechanisms is found over the marine regions adjacent to South Asia (Bay of Bengal and northern Indian Ocean), with MOZART predicting significantly higher 24-h average ozone levels (35-50 ppbv) compared to the RADM2 (25-40 ppbv). A comparison of noontime average ozone distributions between the two chemical mechanism shows that MOZART predicts higher ozone concentrations than RADM2 over most of the Indian region by about 5-20 ppbv, except over western India. The differences are up to 20 ppbv and more over the Southern Indian region, highlighting the impacts of chemical mechanisms on modelled ozone in this region. The mean bias (MB) values (model-observation) for 24-h and noontime average ozone at individual stations is provided in the supplementary material - Table S2 and S3.

Figure 9a shows a comparison of the monthly average chemical  $O_3$  tendency ( $ppbv\ h^{-1}$ ) from 0630 to 1230 IST. In contrast with average  $O_3$  mixing ratios, which were found to be higher in HTAP-MOZ, the net  $O_3$  production rates at the surface are higher in HTAP-RADM2 over most of the domain, especially in the IGP and central India. The net  $O_3$  production rates at the surface with HTAP-RADM2 are found to be 6 to 9  $ppbv\ h^{-1}$  and more over the IGP, whereas these values are generally lower in HTAP-MOZ (4-8  $ppbv\ h^{-1}$ ), except in the north-eastern IGP (>9  $ppbv\ h^{-1}$ ). Fig. 9b shows the sum of the chemical tendency and vertical mixing tendency at the surface for the HTAP-RADM2 and HTAP-MOZ. Analysis of the vertical mixing tendency revealed that higher surface ozone mixing ratios in the MOZART simulation are due to mixing with ozone rich air from aloft. In the HTAP-RADM2



simulation, vertical mixing dilutes the effect of strong chemical surface ozone production. Further analysis of vertical distributions of chemical O<sub>3</sub> tendencies reveals stronger photochemical production of ozone aloft with MOZART compared to RADM2 (Supplementary material-Fig. S7). This leads to higher ozone mixing ratios aloft in MOZART simulations. A sensitivity simulation is conducted using a different PBL parameterization (Yonsei University Scheme) to examine its influence on our conclusions. Comparison of monthly average (in April) planetary boundary layer heights between the two PBL schemes revealed that the differences are mostly within  $\pm 150$  m with Yonsei scheme generally resulting in higher PBL heights over India (Fig. S9). Nevertheless, the chemical tendencies combined with vertical mixing tendencies of surface O<sub>3</sub> are found to be nearly similar with Yonsei scheme (Fig. S10) as in the base runs using the MYJ scheme (Fig. 9b) with MOZART still producing higher ozone aloft (not shown) as in the original runs. Thus changing the PBL scheme still results in production of more ozone aloft in MOZART, which is getting mixed with near surface air, which corroborates that our conclusions are not affected.

Mar et al. (2016) showed that RADM2 exhibits greater VOC sensitivity than MOZART (i.e., producing higher changes in ozone given a perturbation in VOC emissions) under noontime summer conditions over Europe. This is consistent with our findings as well, that the net surface photochemical ozone production is greater for HTAP-RADM2 than for HTAP-MOZART, given the high VOC emissions in the HTAP inventory. At the surface, the MOZART mechanism predicts larger areas of VOC-sensitivity (as diagnosed by the CH<sub>2</sub>O/NO<sub>y</sub> indicator, Figure 10) and lower net photochemical ozone production than RADM2. With increasing altitude, both the HTAP-RADM2 and HTAP-MOZART simulations show a general increase of CH<sub>2</sub>O/NO<sub>y</sub> over India, i.e. the chemistry tends to exhibit increased NO<sub>x</sub> sensitivity with increasing height (Supplementary material-Figure S11). At model levels above the surface, HTAP-MOZART shows greater net photochemical production of ozone than HTAP-RADM2 (Supplementary material-Figure S7), which is what Mar et al. (2016) have also reported for the surface O<sub>3</sub> over Europe. When these effects are combined, mixing leads to higher surface ozone mixing ratios for HTAP-MOZART than for HTAP-RADM2. A sensitivity simulation using a different photolysis scheme (Madronich TUV photolysis scheme) with HTAP-RADM2 setup revealed similar surface ozone mixing ratios and chemical tendencies at various model levels with small differences (<5%) over most of the Indian region (not shown). So our results would be similar if we use Madronich TUV scheme instead of Fast-J scheme with RADM2. Further, Mar et al. (2016) used Madronich TUV scheme with RADM2 and Madronich F-TUV scheme with MOZART chemical mechanism and reported that the two different Madronich photolysis schemes had only a small contribution to the differences in the predicted ozone by two chemical mechanisms. The major difference between the two chemical mechanisms was due to differences in inorganic reaction rates (Mar et al, 2016). Hence we conclude that in our study too, the differences over Indian region are primarily due to the choice of the chemical mechanisms irrespective of photolysis scheme used. Also note that the aerosol radiation feedback is turned off, so that the calculated differences mainly result from the representation of gas phase chemistry rather than of aerosols between MOZART and RADM2. Our analysis also shows the importance of chemical regime in understanding differences between the chemical mechanisms, and highlights the significant effects of the employed chemical mechanism on modelled ozone over South Asia.

## 4.2. Diurnal variation

Figure 11 shows a comparison of WRF-Chem simulated ozone variations on diurnal timescales with recent in situ measurements over a network of stations across the South Asia for the two chemical mechanisms (MOZART and

RADM2); again with the same emission inventory (HTAP). Qualitatively, both simulations produce very similar diurnal patterns (also see Supplementary material, Fig. S12), however, the absolute O<sub>3</sub> mixing ratios are found to differ significantly (Figure 11) between the two chemical mechanisms. Noontime ozone mixing ratios predicted by MOZART are either significantly higher (at 9 out of 15 stations) or nearly similar (at 6 stations). MOZART-predicted O<sub>3</sub> at Dibrugarh, Kanpur, Jabalpur, Bhubaneswar, Gadanki and Thumba was found to be higher by ~12 ppbv, 5 ppbv, 8 ppbv, 10 ppbv, 11 ppbv and 12 ppbv, respectively, compared to RADM2 (Supplementary material, Table S3). Over several urban and rural stations in India (e.g. Delhi, Ahmedabad, Pune, Kannur and Thumba) MOZART is found to titrate ozone more strongly during the night while resulting in higher or similar ozone levels around noon. The contrasting comparison between noon and night time found at these sites suggests that evaluation limited to 24 h averages would not be sufficient, and that model performance on a diurnal time scale should be considered to assess the photochemical build-up of O<sub>3</sub>.

~~In general, the noontime ozone mixing ratios predicted by RADM2 are found to be in better agreement with in situ measurements compared to MOZART.~~ The model performance of two chemical mechanisms in reproducing diurnal variation at all stations is summarised using a Taylor diagram in Fig. 12. Both chemical mechanisms show reasonably good agreement ( $r > 0.7$ ) at most of the sites, except ~~two-one~~ stations associated with highly complex terrain (Nainital ~~and Mt. Abu~~). On the Taylor diagram, most of the HTAP-RADM2 results are found to be closer to the 'REF', as compared to HTAP-MOZ results, suggesting that the RADM2 chemical mechanism is better suited to simulate diurnal variation of ozone over this region.

## 5. Overall evaluation and recommendations

In this section, we present a sub-regional evaluation of all simulations by subdividing the domain into five geographical areas, i.e. North, South, East, West and central India, as shown in Fig. 1. ~~The recommendations for the individual stations based on the model evaluation are summarized in the Supplementary material (Table S2 and S3).~~ The temporal correlation coefficients of diurnally varying O<sub>3</sub>, spatially averaged over each of the five different sub-regions, are found to be reasonably high, generally exceeding 0.7 (Table 5). The  $r$  values for individual sub-regions are found to be similar among the four simulations. For example, over north India the  $r$  values vary from 0.86 to 0.90. The model performance differs among several sub-regions, with correlations being lower for central India ( $r = 0.67$ -0.75). Since the latter is based on only one station associated with complex terrain (Jabalpur), we suggest that observations over additional stations should be conducted to evaluate the model performance in the central Indian region. ~~As correlations are similar among different simulations, we focus on the~~ The mean bias values ~~especially around noontime~~ are provided in supplementary material (Table S5). ~~Amongst the four different combinations of simulations performed we find HTAP-RADM2 yields lowest noontime biases over north (MB = -2.4 ppbv) and central India (-0.9 ppbv). The S4RS-RADM2 combination is recommended for the east (MB = 15.3 ppbv) and South (MB = 6.5 ppbv) Indian regions. On the other hand, INTEX-RADM2 is found to yield better agreement with measurements over western India (MB = -8 ppbv). The recommendation for each region based solely on the ability to predict noontime O<sub>3</sub> concentrations is summarized in table 7.~~ These results show that the performance of emission inventories is regionally different, and that these biases should be considered in utilizing model for assessment of air quality and impacts on human health and crop yield.

We finally evaluate the different simulations in the context of the entire south Asian region. Figure 13 shows a comparison of model results and measurements with diurnal box/whisker plots, combining all stations for the four different simulations. ~~As mentioned earlier, noontime ozone levels are overestimated by all four simulations. The overestimation of noontime ozone is found to be largest in the HTAP-MOZ simulation, followed by HTAP-RADM2, and lowest with S4RS-RADM2. It is clearly seen that HTAP-MOZ yields highest noontime surface ozone mixing ratios among all simulations followed by HTAP-RADM2.~~ These results further suggest that assessment of the tropospheric ozone budget as well as implications for public health and crop loss are associated with considerable uncertainty, and biases need to be considered. A recent study (Ghude et al., 2016) utilizing MOZART chemistry, for example, subtracted 15 ppbv from the WRF-Chem simulated ozone mixing ratios before deriving premature mortalities over the Indian region. The results of present study are summarized in the form of a polar plot (Fig. 14) showing the monthly mean diurnal variation from all runs for the entire south Asian domain. The noontime normalized mean bias values with respect to observed values are ~9.7% (S4RS-RADM2), ~11.5% (INTEX-RADM2), ~20.9% (HTAP-RADM2) and ~34.2% (HTAP-MOZ). ~~It is to be noted that comparison of absolute ozone levels from model with observations has a limitation due to non-consideration of aerosol impacts and the resolution at which the model results are obtained; nevertheless, it provides an estimate about the uncertainties in model predictions of ozone using different emission inventories.~~ It is interesting to note that the SEAC4RS inventory (representative of year 2012) yields quite similar domain wide average bias value as the INTEX-B inventory (representative of year 2006). ~~It is concluded that the SEAC4RS inventory, which is the most recent inventory amongst the three inventories considered in this study, is best suited for O<sub>3</sub> prediction over south Asian region as a whole in combination with RADM2 Chemistry.~~

## 6. Summary and conclusions

In this paper, we ~~evaluated-compare~~ the WRF-Chem simulated surface ozone over South Asia during the pre-monsoon season ~~by against recent in-situ measurements from a network of 18 stations,~~ employing three different inventories (EDGAR-HTAP, INTEX-B, and SEAC4RS) for anthropogenic emissions with the RADM2 chemical mechanism. WRF-Chem simulated ozone distributions showed highest ozone mixing ratios (~55 ppbv and higher) over northern India and the Tibetan Plateau. In general, modelled average ozone distributions from different inventories are found to be in agreement with previous studies over this region. Evaluation on diurnal time scales demonstrates the ability of the model to reproduce observed O<sub>3</sub> patterns at urban and rural stations, showing strong noontime ozone build-up and chemical titration and deposition loss during the night-time. WRF-Chem also captures the smaller diurnal amplitudes observed over high altitude, relatively pristine stations. However, model showed limitations in capturing ozone mixing ratios in the vicinity of the complex terrain, indicating that even a relatively high horizontal resolution of 12 km x 12 km could not fully resolve the topography induced effects.

Overall WRF-Chem simulations show reasonable agreement with observations, with correlation coefficients generally higher than 0.7 for most of the sites. It is found that the HTAP, INTEX-B and SEAC4RS inventories lead to very similar distributions of 24-h average ozone over this region. This is corroborated by the quantitative similarity in simulated surface ozone among the three simulations, for both 24h and noontime (1130-1630 IST) averages at all grids in the domain (supplementary material, table S6). However, noontime (1130-1630 IST) O<sub>3</sub> mixing ratios over continental South Asia differ significantly among the three inventories. This can also be seen in the quantitative assessment of similarity (Table S6), where the variance of the residual shows that the scatter is

greater for the noontime averages than for the 24 h averages. HTAP inventory generally leads to noontime O<sub>3</sub> mixing ratios higher by 10 ppbv over the Indo-Gangetic plain (IGP), 20 ppbv over Central India, and 30 ppbv over Southern India, compared to the INTEx-B and SEAC4RS inventories. A comparison of monthly average O<sub>3</sub> net production rate during 0630-1230 IST among the three inventories shows that the HTAP emissions result in faster O<sub>3</sub> production (~9 ppbv h<sup>-1</sup>) throughout the IGP region compared to the other two inventories. Differences are also found over the southern Indian region with stronger ozone production in HTAP, followed by INTEx-B and SEAC4RS. The results show similar 24-h average ozone distributions, but large differences in noontime ozone build up, pointing to the uncertainties in emission inventories over this region.

We further investigated the sensitivity of modelled ozone to two extensively used chemical mechanisms, RADM2 and MOZART, and maintaining the HTAP emissions. Noontime average surface ozone distributions predicted by MOZART show significant enhancements (10-15 ppbv) with respect to RADM2 over most of the Indian region, except over western India. MOZART predicts higher ozone concentrations than RADM2 by up to 20 ppbv and more over the South Indian region. Monthly average ozone mixing ratios are predicted to be higher by the MOZART chemical mechanism compared to RADM2, as was also found over Europe (Mar et al., 2016). The differences in ozone production between the MOZART and RADM2 chemical mechanisms are mainly attributed to the additional chemical species and reactions, differences in the rate constants for several inorganic reactions, and photolysis schemes used. [The difference in photolysis rates for O<sup>1</sup>D and NO<sub>2</sub> can be seen in supplementary material \(Figure S13\) for a surface point in the centre of the domain.](#) A comparison of the monthly average chemical O<sub>3</sub> tendency (ppbv h<sup>-1</sup>) during 0630-1230 IST shows that in contrast with average O<sub>3</sub> mixing ratios, which were found to be higher in MOZART, the net O<sub>3</sub> production rates at the surface are higher with RADM2 chemistry, especially over the IGP and central India. The net O<sub>3</sub> production rates at the surface with RADM2 are found to be 6 to 9 ppbv h<sup>-1</sup>, and higher over the IGP, whereas these rates are generally lower with MOZART (4-8 ppbv h<sup>-1</sup>), except in the northeastern IGP (>9 ppbv h<sup>-1</sup>). Analysis of the vertical mixing tendency revealed that higher surface ozone mixing ratios in the MOZART simulation are due to mixing with ozone rich air from aloft. Analysis of vertical distributions of chemical O<sub>3</sub> tendencies reveals stronger photochemical production of ozone aloft with MOZART compared to RADM2. Our analysis highlights the significant effects of the employed chemical mechanism on model predicted ozone over South Asia.

Qualitatively, RADM2 and MOZART simulations predict similar diurnal patterns ~~\_; however the absolute O<sub>3</sub> mixing ratios differ significantly. Noontime ozone mixing ratios predicted by MOZART are significantly higher at 9 out of 15 stations, while these were found to be similar at 6 stations. However,~~ over several urban and rural stations in India MOZART is found to titrate ozone relatively strongly during the night, while producing higher or similar ozone levels during noontime compared to RADM2. The contrasting evaluation results between day- (noon) and night-time could counterbalance in evaluation studies limited to 24 h averages, possibly showing better agreement and therefore it is pertinent to consider the diurnally resolved model performance. ~~In general, the noontime ozone mixing ratios predicted by RADM2 are found to be in better agreement with in situ measurements at the surface compared to MOZART.~~

~~Model evaluation over different geographical regions in South Asia reveals strong spatial heterogeneity in the WRF-Chem performance. SEAC4RS inventory leads to better agreement with observations over east (MB = ~15.3 ppbv) and south India (~6.5 ppbv), whereas the HTAP inventory performs better over north (MB = ~2.4 ppbv) and~~

central India ( $\sim 0.9$  ppbv), and INTEX-B over west India ( $MB = \sim 8$  ppbv). For the entire region, the overestimation of noontime ozone is found to be highest with the HTAP inventory (with the MOZART chemical mechanism) and lowest with the SEAC4RS inventory. Model results averaged over all observation sites encompassing the South Asian region revealed that HTAP-MOZ predicts highest noontime ozone mixing ratios followed by HTAP-RADM2. The noontime normalized mean bias compared to observations is lowest for the SEAC4RS inventory with the RADM2 chemical mechanism ( $\sim 9.7\%$ ), followed by INTEX-B with RADM2 ( $\sim 11.5\%$ ), HTAP with RADM2 ( $\sim 20.9\%$ ), and HTAP with MOZART ( $\sim 34.2\%$ ). These results further suggest that the assessment of the tropospheric ozone budget and consequently its implications on public health and agricultural output should be carried out cautiously by considering the large uncertainties associated with use of emission inventories and chemical mechanism incorporated. As we report considerable differences in the noontime ozone levels among different inventories, further work is needed to account for aerosol feedback, and evaluation of ozone precursors to identify best suited emission inventory for this region. It is interesting to note that the SEAC4RS inventory (representative of 2012) yields results comparable to the INTEX-B inventory (for 2006), even though the SEAC4RS inventory has about 46% higher  $NO_x$ , 9% higher NMVOC and 15% lower CO emissions compared to INTEX-B. We conclude that the SEAC4RS inventory, the most recent inventory amongst the three inventories, is best suited for  $O_3$  prediction over south Asian region as a whole in combination with RADM2 Chemistry.

Brown carbon aerosol can effectively absorb solar radiation (Alexander et al., 2008; Hecobian et al., 2010; Kirchstetter and Thatcher, 2012; Kirchstetter et al., 2004; Yang et al., 2009; Jo et al., 2016) leading to a reduction in  $NO_2$  photolysis rates and subsequently in surface ozone mixing ratios (Jo et al., 2016). Jo et al. (2016) reported that on an annual average basis, changes in surface ozone mixing ratios related to brown carbon aerosol absorption over South Asia are  $<5\%$ . Further studies should be taken up in the future to investigate the impact of aerosols on surface ozone, also with regional models like WRF-Chem. The current and other modelling efforts, constrained by limited measurement data, stress the need for more comprehensive observations, e.g. in a network of stations, and making the data available through projects such as TOAR (<http://toar-data.fz-juelich.de/>). Our study highlights the need to also evaluate  $O_3$  precursors, similar to that conducted here for ozone, to further reduce uncertainties in modelled ozone over South Asia for the better assessment of implications of surface ozone on public health and crop yield. In order to make better model predictions at further higher resolution (than 12 km), development of finer resolution inventories than the ones used in the current study is also required over the region. So we also recommend preparing high-resolution regional inventories for the anthropogenic emissions of  $O_3$  precursors over South Asia, also accounting for year-to-year changes.

**Data availability:** The model output from all the numerical simulations is available at the MPG supercomputer HYDRA (<http://www.mpcdf.mpg.de/services/computing/hydra>) and would be provided by contacting the corresponding authors. The observed values shown for comparison are from previous papers with complete list of references provided in the Table 4. New observations for Delhi and Pune stations are available from the SAFAR program (<http://safar.tropmet.res.in/>).

## Acknowledgement

A. Sharma acknowledges the fellowship from the Max Planck Institute for Chemistry to carry out this study. S. S. Gunthe acknowledges the support from DST-Max Planck partner group at IIT Madras and Ministry of Earth

Sciences (MoES), Govt. of India. Model simulations have been performed on the MPG supercomputer HYDRA (<http://www.mpcdf.mpg.de/services/computing/hydra>). Initial and boundary conditions data for meteorological fields were obtained from ECMWF website (<http://www.ecmwf.int/en/research/climate-reanalysis/era-interim>). The HTAP v2 anthropogenic emissions were obtained from [http://edgar.jrc.ec.europa.eu/htap\\_v2/index.php?SECURE=123](http://edgar.jrc.ec.europa.eu/htap_v2/index.php?SECURE=123). Authors are grateful to Yafang Cheng (MPI-C) for providing SEAC4RS emission. The INTEX-B anthropogenic emissions were obtained from [http://bio.cgrer.uiowa.edu/EMISSION\\_DATA\\_new/data/intex-b\\_emissions/](http://bio.cgrer.uiowa.edu/EMISSION_DATA_new/data/intex-b_emissions/). MOZART-4/ GEOS5 output used as initial and boundary conditions for chemical fields is acknowledged. The pre-processors and inputs for biogenic and biomass-burning emissions were obtained from NCAR Atmospheric Chemistry website (<http://www.acd.ucar.edu/wrf-chem/>). Radiosonde data of water vapour mixing ratio, temperature and wind speed were obtained from University of Wyoming website (<http://weather.uwyo.edu/upperair/sounding.html>). Authors are also thankful for the usage of HPC supercluster and to the staff at P. G. Senapathy Computer Center at IIT Madras. Constructive comments and suggestions from two anonymous reviewers are gratefully acknowledged.

## References

- Ackermann, I. J., Hass, H., Memmesheimer, M., Ebel, A., Binkowski, F. S., and Shankar, U.: Modal aerosol dynamics model for Europe: development and first applications, *Atmos. Environ.*, 32, 2981–2999, doi:10.1016/S1352-2310(98)00006-5, 1998.
- Ainsworth, E. A., Yendrek, C. R., Sitch, S., Collins, W. J., and Emberson, L. D.: The effects of tropospheric ozone on net primary productivity and implications for climate change, *Ann. Rev. Plant Biol.*, 63, 637–661, 2012.
- Akimoto, H.: Global air quality and pollution, *Science*, 302, 1716–1719, doi:10.1126/science.1092666, 2003.
- Alexander, D. T. L., Crozier, P. A., and Anderson, J. R.: Brown carbon spheres in East Asian outflow and their optical properties, *Science*, 321, 833–836, doi:10.1126/science.1155296, 2008.
- Amnuaylojaroen, T., Barth, M. C., Emmons, L. K., Carmichael, G. R., Kreasuwun, J., Prasitwattanaseree, S., and Chantara, S.: Effect of different emission inventories on modeled ozone and carbon monoxide in Southeast Asia, *Atmos. Chem. Phys.*, 14, 12983–13012, doi:10.5194/acp-14-12983-2014, 2014.
- Anenberg, S. C., Horowitz, L. W., Tong, D. Q., and West, J. J.: An estimate of the global burden of anthropogenic ozone and fine particulate matter on premature human mortality using atmospheric modelling, *Environmental Health Perspectives*, 118, 1189–1195, 2010.
- Ansari, T. U., Ojha, N., Chandrasekar, R., Balaji, C., Singh, N. and Gunthe, S. S.: Competing impact of anthropogenic emissions and meteorology on the distribution of trace gases over Indian region, *J. Atmos. Chem.*, doi:10.1007/s10874-016-9331-y, 2016.
- Atkinson, R.: Atmospheric chemistry of VOCs and NO<sub>x</sub>, *Atmos. Environ.*, 34, 2063–2101, doi:10.1016/S1352-2310(99)00460-4, 2000.
- Barth, M. C., Lee, J., Hodzic, A., Pfister, G., Skamarock, W. C., Worden, J., Wong, J., and Noone, D.: Thunderstorms and upper troposphere chemistry during the early stages of the 2006 North American Monsoon, *Atmos. Chem. Phys.*, 12, 11003–11026, doi:10.5194/acp-12-11003-2012, 2012.

632 Beig, G., Gunthe, S., and Jadhav, D. B.: Simultaneous measurements of ozone and its precursors on a diurnal scale  
633 at a semi urban site in India, JOURNAL OF ATMOSPHERIC CHEMISTRY, 57, 239-253, doi: 10.1007/s10874-  
634 007-9068-8, 2007.

635 Bell, M. L., McDermott, A., Zeger, S. L., Samet, J. M., and Dominici, F.: Ozone and short term mortality in 95 US  
636 urban communities, 1987-2000, JAMA The Journal of the American Medical Association, 292, 2372-2378, 2004.

637 Bhuyan, P.K., Bharali, C., Pathak, B., and Kalita, G.: The role of precursor gases and meteorology on temporal  
638 evolution of O<sub>3</sub> at a tropical location in northeast India, Environmental Science and Pollution Research, 21, 6696–  
639 6713, 2014.

640 Carmichael, G. R., Sakurai, T., Streets, D., Hozumi, Y., Ueda, H., Park, S. U., Funge, C., Han, Z., Kajino, M.,  
641 Engardt, M., Bennet, C., Hayami, H., Sartelet, K., Holloway, T., Wang, Z., Kannari, A., Fu, J., Matsuda, K.,  
642 Thongboonchoo, N., and Amann, M.: MICS-Asia II: the model intercomparison study for Asia Phase II  
643 methodology and overview of findings, Atmos. Environ., 42, 3468–3490, doi:10.1016/j.atmosenv.2007.04.007,  
644 2008.

645 Chin, M., Rood, R. B., Lin, S. -J., Muller, J. F., and Thompson, A. M.: Atmospheric sulfur cycle in the global  
646 model GOCART: Model description and global properties, J. Geophys. Res., 105, 24,671-24,687, 2000.

647 Chou, M. -D., and Suarez, M. J.: An efficient thermal infrared radiation parameterization for use in general  
648 circulation models, NASA Technical Memorandum 104606, 3, 85pp, 1994.

649 Cox, R. A., Eggleton, A. E. J., Derwent, R. G., Lovelock, J. E., and Pack, D. H.: Long-range transport of  
650 photochemical ozone in north-western Europe, Nature, 255, 118 – 121, doi:10.1038/255118a0, 1975.

651 Crutzen, P. J.: Photochemical reactions initiated by and influencing ozone in unpolluted tropospheric air, Tellus,  
652 26, 47–57, 1974.

653 David, L. M., and Nair, P. R.: Diurnal and seasonal variability of surface ozone and NO<sub>x</sub> at a tropical coastal site:  
654 association with mesoscale and synoptic meteorological conditions, Journal of Geophysical Research 116,  
655 D10303. <http://dx.doi.org/10.1029/2010JD015076>, 2011.

656 ~~Debaje, S. B., and Kakade, A. D.: Measurements of Surface Ozone in Rural Site of India, Aerosol and Air Quality~~  
657 ~~Research, Vol. 6, No. 4, pp. 444-465, 2006.~~

658 Dumka, U. C., Krishna Moorthy, K., Kumar, R., Hegde, P., Sagar, R., Pant, P., Singh, N., and Suresh Babu, S.:  
659 Characteristics of aerosol black carbon mass concentration over a high altitude location in the central Himalayas  
660 from multi-year measurements, Atmos. Res., 96, 510–521, 2010.

661 Emberson, L. D., Buker, P., Ashmore, M., Mills, G., Jackson, L., Agrawal, M., Atikuzzaman, M., Cinderby, S.,  
662 Engardt, M., Jamir, C., Kobayashi, K., Oanh, N., Quadir, Q., and Wahid, A.: A comparison of North -American  
663 and Asian exposure-response data for ozone effects on crop yields, Atmos. Environ., 43, 1945–1953, 2009.

664 Emmons, L. K., Walters, S., Hess, P. G., Lamarque, J.-F., Pfister, G. G., Fillmore, D., Granier, C., Guenther, A.,  
665 Kinnison, D., Laepple, T., Orlando, J., Tie, X., Tyndall, G., Wiedinmyer, C., Baughcum, S. L., and Kloster, S.:

666 Description and evaluation of the Model for Ozone and Related chemical Tracers, version 4 (MOZART-4),  
 667 Geosci. Model Dev., 3, 43–67, 20 doi:10.5194/gmd-3-43-2010, 2010.

668 Fast, J. D., Gustafson Jr., W. I., Easter, R. C., Zaveri, R. A., Barnard, J. C., Chapman, E. G., Grell, G. A. and  
 669 Peckham, S. E.: Evolution of ozone, particulates, and aerosol direct radiative forcing in the vicinity of Houston  
 670 using a fully-coupled meteorology-chemistry aerosol model, *Journal of Geophysical Research*, 111, D21305,  
 671 2006.

672 Gaur, A., Tripathi, S. N., Kanawade, V. P., Tare, V., and Shukla, S. P.: Four-year measurements of trace gases  
 673 (SO<sub>2</sub>, NO<sub>x</sub>, CO, and O<sub>3</sub>) at an urban location, Kanpur, in Northern India, *J. Atmos. Chem.*, 71, 283–301, 2014.

674 Geng, F., Zhao, C., Tang, X., Lu, G., and Tie, X.: Analysis of ozone and VOCs measured in Shanghai: A case  
 675 study, *Atmos. Environ.*, 41, 989–1001, 2007.

676 Ghude, S. D., Jena, C., Chate, D. M., Beig, G., Pfister, G. G., Kumar, R., and Ramanathan, V.: Reduction in  
 677 India's crop yield due to ozone, *Geophys. Res. Lett.*, 41, 51971, doi:10.1002/2014GL060930, 2014.

678 Ghude, S. D., Chate, D. M., Jena, C., Beig, G., Kumar, R., Barth, M. C., Pfister, G. G., Fadnavis, S. and Pithani,  
 679 P.: Premature mortality in India due to PM<sub>2.5</sub> and ozone exposure, *Geophysical Research Letters*, 4650 – 4658,  
 680 2016.

681 Girach, I. A., Ojha, N., Nair, P. R., Pozzer, A., Tiwari, Y. K., Kumar, K. R., and Lelieveld, J.: Variations in O<sub>3</sub>,  
 682 CO, and CH<sub>4</sub> over the Bay of Bengal during the summer monsoon season: shipborne measurements and model  
 683 simulations, *Atmos. Chem. Phys.*, 17, 257–275, doi:10.5194/acp-17-257-2017, 2017.

684 Grell, G.: Prognostic evaluation of assumptions used by cumulus parameterizations, *Monthly Weather Review*,  
 685 121, 764–787, 1993.

686 Grell, G., and Devenyi, D.: A generalized approach to parameterizing convection combining ensemble and data  
 687 assimilation techniques, *Geophys. Res. Lett.*, 29(14), 38–31, 2002.

688 Grell, G. A., Peckham, S. E., McKeen, S., Schmitz, R., Frost, G., Skamarock, W. C. and Eder, B.: Fully coupled  
 689 'online' chemistry within the WRF model, *Atmospheric Environment*, 39, 6957–6975, 2005.

690 Gupta, M. and Mohan, M.: Validation of WRF/Chem model and sensitivity of chemical mechanisms to ozone  
 691 simulation over megacity Delhi, *Atmospheric Environment*, Volume 122, p. 220–229, 2015.

692 Guenther, A., Karl, T., Harley, P., Wiedinmyer, C., Palmer, P. I., and Geron, C.: Estimates of global terrestrial  
 693 isoprene emissions using MEGAN (Model of Emissions of Gases and Aerosols from Nature), *Atmos. Chem.*  
 694 *Phys.*, 6, 3181–3210, doi:10.5194/acp-6-3181-2006, 2006.

695 Gurjar, B. R., Ravindra, K., and Nagpure, A.S.: Air pollution trends over Indian megacities and their local-to-  
 696 global implications, *Atmospheric Environment*, Volume 142, Pages 475–495,  
 697 <http://dx.doi.org/10.1016/j.atmosenv.2016.06.030>, 2016.



698 Hecobian, A., Zhang, X., Zheng, M., Frank, N., Edgerton, E. S., and Weber, R. J.: Water-Soluble Organic Aerosol  
699 material and the light-absorption characteristics of aqueous extracts measured over the Southeastern United States,  
700 *Atmos. Chem. Phys.*, 10, 5965–5977, doi:10.5194/acp-10-5965-2010, 2010.

701 Jain, S. L., Arya, B. C., Kumar, A., Ghude, S. D., and Kulkarni, P. S.: Observational study of surface ozone at  
702 New Delhi, India, *Int. J. Remote Sens.*, 26, 3515–3524, 2005.

703 Janjic, Z. I.: The step-mountain eta coordinate model: further developments of the convection, viscous sublayer  
704 and turbulence closure schemes, *Monthly Weather Review* 122, 927–945, 1994.

705 Janjic, Z. I.: The surface layer in the NCEP Eta Model, Eleventh Conference on Numerical Weather Prediction,  
706 Norfolk, VA, 19–23 August; American Meteorological Society, Boston, MA, 354–355, 1996.

707 Janjic, Z. I.: Nonsingular Implementation of the Mellor–Yamada Level 2.5 Scheme in the NCEP Meso model,  
708 NCEP Office Note, No. 437, 61 pp, 2002.

709 Janssens-Maenhout, G., Crippa, M., Guizzardi, D., Dentener, F., Muntean, M., Pouliot, G., Keating, T., Zhang, Q.,  
710 Kurokawa, J., Wankmüller, R., Denier van der Gon, H., Kuenen, J. J. P., Klimont, Z., Frost, G., Darras, S., Koffi,  
711 B., and Li, M.: HTAP\_v2.2: a mosaic of regional and global emission grid maps for 2008 and 2010 to study  
712 hemispheric transport of air pollution, *Atmos. Chem. Phys.*, 15, 11411e11432, [http://dx.doi.org/10.5194/acp-15-](http://dx.doi.org/10.5194/acp-15-11411-2015)  
713 11411-2015, 2015.

714 Jena, C., Ghude, S. D., Pfister, G. G., Chate, D. M., Kumar, R., Beig, G., Surendran, D., Fadnavis, S., and Lal, D.  
715 M.: Influence of springtime biomass burning emissions in South Asia on regional ozone: A model based case  
716 study, *Atmos. Environ.*, 100, 37–47, doi:10.1016/j.atmosenv.2014.10.027, 2014.

717 Jena, C., Ghude, S. D., Beig, G., Chate, D. M., Kumar, R., Pfister, G. G., Lal, D. M., Surendran, D. E., Fadnavis,  
718 S., and van der, A. R. J.: Inter-comparison of different NO<sub>x</sub> emission inventories and associated variation in  
719 simulated surface ozone in Indian region, *Atmos. Environ.*, 117:61–73, 2015.

720 Jerrett, M., Burnett, R. T., Pope, C. A., III, Ito, K., Thurston, G., Krewski, D., et al.: Long-term ozone exposure  
721 and mortality, *The New England Journal of Medicine*, 360, 1085–1095, 2009.

722 Jo, D. S., Park, R. J., Lee, S., Kim, S.-W., and Zhang, X.: A global simulation of brown carbon: implications for  
723 photochemistry and direct radiative effect, *Atmos. Chem. Phys.*, 16, 3413–3432, doi:10.5194/acp-16-3413-2016,  
724 2016.

725 Kirchstetter, T. W., Novakov, T., and Hobbs, P. V.: Evidence that the spectral dependence of light absorption by  
726 aerosols is affected by organic carbon, *J. Geophys. Res.*, 109, D21208, doi:10.1029/2004JD004999, 2004.

727 Kirchstetter, T. W. and Thatcher, T. L.: Contribution of organic carbon to wood smoke particulate matter  
728 absorption of solar radiation, *Atmos. Chem. Phys.*, 12, 6067–6072, doi:10.5194/acp-12-6067-2012, 2012.

729 Kleinman, L., Lee, Y. -N., Springston, S. R., Nunnermacker, L., Zhou, X., Brown, R., Hallock, K., Klotz, P.,  
730 Leahy, D., Lee, J. H., and Newman, L.: Ozone formation at a rural site in the southeastern United States, *J.*  
731 *Geophys. Res.-Atmos.*, 99, 3469–3482, doi:10.1029/93JD02991, 1994.

732 [Kleinman L. I., Daum, P. H., Lee, Y.-N., Nunnermacker, L. J., Springston, S. R., Weinstein-Lloyd, J., Hyde, P.,](#)  
 733 [Doskey, P., Rudolph, J., Fast, J., and Berkowitz, C.: Photochemical age determinations in the Phoenix](#)  
 734 [metropolitan area, J. Geophys. Res.,108, 4096, doi:10.1029/2002JD002621, 2003.](#)

735 Krupa, S. V., Nosal, M., and Legge, A. H.: A numerical analysis of the combined open top chamber data from the  
 736 USA and Europe on ambient ozone and negative crop responses, *Environmental Pollution*, 101, 157–160, 1998.

737 Kumar, R., Naja, M., Venkataramani, S., and Wild, O.: Variations in surface ozone at Nainital: A high-altitude site  
 738 in the central Himalayas, *J. Geophys. Res.*, 115, D16302, doi:10.1029/2009JD013715, 2010.

739 Kumar, R., Naja, M., Pfister, G. G., Barth, M. C., and Brasseur, G. P.: Simulations over South Asia using the  
 740 Weather Research and Forecasting model with Chemistry (WRF-Chem): set-up and meteorological evaluation,  
 741 *Geoscientific Model Development*, 5, 321-343, 2012a.

742 Kumar, R., Naja, M., Pfister, G. G., Barth, M. C., Wiedinmyer, C., and Brasseur, G. P.: Simulations over South  
 743 Asia using the Weather Research and Forecasting model with Chemistry (WRF-Chem): chemistry evaluation and  
 744 initial results, *Geoscientific Model Development* 5, 619-648, 2012b.

745 Kumar, R., Barth, M. C., Pfister, G. G., Nair, V. S., Ghude, S. D., and Ojha, N.: What controls the seasonal cycle  
 746 of black carbon aerosols in India?, *J. Geophys. Res. Atmos.*, 120, 7788–7812, doi:10.1002/2015JD023298, 2015.

747 Lawrence, M. G., Rasch, P. J., von Kuhlmann, R., Williams, J., Fischer, H., de Reus, M., Lelieveld, J., Crutzen, P.  
 748 J., Schultz, M., Stier, P., Huntrieser, H., Heland, J., Stohl, A., Forster, C., Elbern, H., Jakobs, H., and Dickerson,  
 749 R. R.: Global chemical weather forecasts for field campaign planning: predictions and observations of large-scale  
 750 features during MINOS, CONTRACE, and INDOEX, *Atmos. Chem. Phys.*, 3, 267-289, doi:10.5194/acp-3-267-  
 751 2003, 2003.

752 Lawrence, M. G. and Lelieveld, J.: Atmospheric pollutant outflow from southern Asia: a review, *Atmos. chem.*  
 753 *Phys.*, 10, 11017–11096, doi:10.5194/acp-10-11017-2010, 2010.

754 Lelieveld, J., and Dentener, F.J.: What controls tropospheric ozone?, *J. Geophys. Res.*, 105, 3531-3551, 2000.

755 Lelieveld, J., Berresheim, H., Borrmann, S., Crutzen, P. J., Dentener, F. J., Fischer, H., Feichter, J., Flatau, P. J.,  
 756 Heland, J., Holzinger, R., Korrman, R., Lawrence, M. G., Levin, Z., Markowicz, K. M., Mihalopoulos, N.,  
 757 Minikin, A., Ramanathan, V., de Reus, M., Roelofs, G. J., Scheeren, H. A., Sciare, J., Schlager, H., Schultz, M.,  
 758 Siegmund, P., Steil, B., Stephanou, E. G., Stier, P., Traub, M., Warneke, C., Williams, J., and Ziereis, H.: Global  
 759 air pollution crossroads over the Mediterranean, *Science*, 298, 794–799, doi:10.1126/science.1075457, 2002.

760 Lelieveld, J., Evans, J. S., Fnais, M., Giannadaki, D., and Pozzer, A.: The contribution of outdoor air pollution  
 761 sources to premature mortality on a global scale, *Nature*, 525(7569):367-371, 2015.

762 Lin, Y.-L., R. D. Farley, R. D. and Orville, H. D.: Bulk parameterization of the snow field in a cloud model, *J.*  
 763 *Clim. Appl. Meteorol.*, 22, 1065–1092, 1983.

764 Liu, Y., Warner, T. T., Bowers, J. F., Carson, L. P., Chen, F., Clough, C. A., Davis, C. A., Egeland, C. H.,  
 765 Halvorson, S., Huck Jr., T. W., Lachapelle, L., Malone, R. E., Rife, D. L., Sheu, R., -S., Swerdlin, S. P. and

766 Weingarten, D. S.: The operational mesogamma-scale analysis and forecast system of the U.S. Army Test and  
 767 Evaluation Command. Part 1: Overview of the modeling system, the forecast products, *Journal of applied*  
 768 *meteorology and climatology* 47, 1077–1092, 2008.

769 Logan, J. A., Staehelin, J., Megretskaia, I. A., Cammas, J.-P., Thouret, V., Claude, H., De Backer, H., Steinbacher,  
 770 M., Scheel, H.-E., Stubi, R., Frohlich, M., and Derwent, R.: Changes in ozone over Europe: Analysis of ozone  
 771 measurements from sondes, regular aircraft (MOZAIC) and alpine surface sites, *J. Geophys. Res.*, 117, D09301,  
 772 doi:10.1029/2011JD016952, 2012.

773 Lu, Z. and Streets, D. G.: The Southeast Asia Composition, Cloud, Climate Coupling Regional Study Emission  
 774 Inventory, available at: <http://bio.cgrer.uiowa.edu/SEAC4RS/emission.html>, 2012.

775 Lüthi, Z. L., Skerlak, B., Kim, S.-W., Lauer, A., Mues, A., Rupakheti, M., and Kang, S.: Atmospheric brown  
 776 clouds reach the Tibetan Plateau by crossing the Himalayas, *Atmos. Chem. Phys.*, 15, 6007–6021,  
 777 doi:10.5194/acp-15-6007-2015, 2015.

778 Mahapatra, P. S., Jena, J., Moharana, S., Srichandan, H., Das, T., Roy, C. G., and Das, S. N.: Surface ozone  
 779 variation at Bhubaneswar and intra-corelationship study with various parameters, *J. Earth Syst. Sci.* 121, 1163–  
 780 1175, 2012.

781 Mallik C., Lal, S., and Venkataramani, S.: Trace gases at a semi-arid urban site in western India: variability and  
 782 inter-correlations, *J. Atm. Chem.* Vol. 72, p. 143–164, 2015.

783 Mar, K. A., Ojha, N., Pozzer, A., and Butler, T. M.: Ozone air quality simulations with WRF-Chem (v3.5.1) over  
 784 Europe: model evaluation and chemical mechanism comparison, *Geosci. Model Dev.*, 9, 3699–3728,  
 785 doi:10.5194/gmd-9-3699-2016, 2016.

786 Marrapu, P., Cheng, Y., Beig, G., Sahu, S. K., Srinivas, R. and Carmichael, G. R.: Air Quality in Delhi during the  
 787 Commonwealth Games, *Atmos. Chem. Phys.*, 14:10619–10630, 2014.

788 Mellor, G. L., and Yamada, T.: Development of a turbulence closure model for geophysical fluid problems,  
 789 *Reviews of geophysics and space physics* 20(4), 851–875, 1982.

790 Michael, M., Yadav, A., Tripathi, S. N., Kanawade, V. P., Gaur, A., Sadavarte, P. and Venkataraman, C.:  
 791 Simulation of trace gases and aerosols over the Indian Domain: Evaluation of the WRF-Chem model, *Atmospheric*  
 792 *Chemistry and Physics Discussion*, 13, 12287–12336, 2013.

793 Mlawer, E. J., Taubman, S. J., Brown, P. D., Iacono, M. J. and Clough, S. A.: Radiative transfer for  
 794 inhomogeneous atmosphere: RRTM, a validated correlated-k model for the long-wave, *Journal of Geophysical*  
 795 *Research* 102 (D14), 16663–16682, 1997.

796 Monin, A. S. and Obukhov, A. M.: Basic laws of turbulent mixing in the surface layer of the atmosphere, *Contrib.*  
 797 *Geophys. Inst. Acad. Sci., USSR* 24 (151), 163–187, 1954.

798 Monks, P. S., Archibald, A. T., Colette, A., Cooper, O., Coyle, M., Derwent, R., Fowler, D., Granier, C., Law, K.  
 799 S., Mills, G. E., Stevenson, D. S., Tarasova, O., Thouret, V., von Schneidmesser, E., Sommariva, R., Wild, O.,

and Williams, M. L.: Tropospheric ozone and its precursors from the urban to the global scale from air quality to short-lived climate forcer, *Atmos. Chem. Phys.*, 15, 8889–8973, doi:10.5194/acp-15-8889-2015, 2015.

~~Naja, M., Lal, S., and Chand, D.: Diurnal and seasonal variabilities in surface ozone at a high altitude site Mt Abu (24.6N, 72.7E, 1680 m asl) in India, *Atmospheric Environment* 37, 4205–4215, 2003.~~

Nishanth, T., Praseed, K. M., Satheesh Kumar, M. K., and Valsaraj, K. T.: Analysis of Ground Level O<sub>3</sub> and NO<sub>x</sub> Measured at Kannur, India. *J Earth Sci Climate Change*, 3:111, doi:10.4172/2157-7617.1000111, 2012.

Ohara, T., Akimoto, H., Kurokawa, J., Horii, N., Yamaji, K., Yan, X., and Hayasaka, T.: An Asian emission inventory of anthropogenic emission sources for the period 1980–2020, *Atmos. Chem. Phys.*, 7, 4419–4444, doi:10.5194/acp-7-4419-2007, 2007.

Ojha, N., Naja, M., Singh, K. P., Sarangi, T., Kumar, R., Lal, S., Lawrence, M. G., Butler, T. M., and Chandola, H. C.: Variabilities in ozone at a semi-urban site in the Indo-Gangetic Plain region: Association with the meteorology and regional process, *J. Geophys. Res.*, 117, D20301, doi:10.1029/2012JD017716, 2012.

Ojha, N., Naja, M., Sarangi, T., Kumar, R., Bhardwaj, P., Lal, S., Venkataramani, S., Sagar, R., Kumar, A., and Chandola, H. C.: On the processes influencing the vertical distribution of ozone over the central Himalayas: Analysis of yearlong ozonesonde observations, *Atmos. Environ.*, 88, 201–211, doi:10.1016/j.atmosenv.2014.01.031, 2014.

Ojha, N., Pozzer, A., Rauthe-Schöch, A., Baker, A. K., Yoon, J., Brenninkmeijer, C. A. M., and Lelieveld, J.: Ozone and carbon monoxide over India during the summer monsoon: regional emissions and transport, *Atmos. Chem. Phys.*, 16, 3013–3032, doi:10.5194/acp-16-3013-2016, 2016.

Otte, T. L.: The impact of nudging in the meteorological model for retrospective air quality simulations. Part I: Evaluation against national observation networks, *J. Appl. Meteor. Climatol.*, 47, 1853–1867, 2008.

Pozzer, A., Zimmermann, P., Doering, U. M., van Aardenne, J., Tost, H., Dentener, F., Janssens-Maenhout, G., and Lelieveld, J.: Effects of business-as-usual anthropogenic emissions on air quality, *Atmos. Chem. Phys.*, 12, 6915–6937, doi:10.5194/acp-12-6915-2012, 2012.

Reddy, B. S. K., Kumar, K. R., Balakrishnaiah, G., Gopal, K. R., Reddy, R. R., Ahammed, Y. N., Narasimhulu, K., Reddy, L. S. S., and Lal, S.: Observational studies on the variations in surface ozone concentration at Anantapur in southern India, *Atmos. Res.* 98, 125–139, 2010.

Renuka, K., Gadhavi, H., Jayaraman, A., Lal, S., Naja, M., and Rao, S.: Study of Ozone and NO<sub>2</sub> over Gadanki – a rural site in South India, *J. Atmos. Chem.*, 71, 95–112, doi:10.1007/s10874-014-9284-y, 2014.

Sarangi, T., Naja, M., Ojha, N., Kumar, R., Lal, S., Venkataramani, S., Kumar, A., Sagar, R., and Chandola, H. C.: First simultaneous measurements of ozone, CO and NO<sub>y</sub> at a high altitude regional representative site in the central Himalayas, *J. Geophys. Res.-Atmos.*, 119, 1592–1611, doi:10.1002/2013JD020631, 2014.

833 [Sarkar, M., Venkataraman, C., Guttikunda, S., and Sadavarte, P.: Indian emissions of technology-linked NM VOCs](#)  
834 [with chemical speciation: An evaluation of the SAPRC99 mechanism with WRF-CAMx simulations, Atmospheric](#)  
835 [Environment, 134, 70-83, <http://dx.doi.org/10.1016/j.atmosenv.2016.03.037>, 2016.](#)

836 Sarkar, S., Srivastava, R. K., and Sagar, K.: Diurnal Monitoring Of Surface Ozone And PM2.5 Concentration  
837 And Its Correlation With Temperature, INTERNATIONAL JOURNAL OF TECHNOLOGY ENHANCEMENTS  
838 AND EMERGING ENGINEERING RESEARCH, VOL 3, ISSUE 09, ISSN 2347-4289, 2015.

839 Schell, B., Ackermann, I. J., Hass, H., Binkowski, F. S., and Ebel, A.: Modeling the formation of secondary  
840 organic aerosol within a comprehensive air quality model system, J. Geophys. Res.-Atmos., 106, 28275–28293,  
841 doi:10.1029/2001JD000384, 2001.

842 Sillman, S.: The use of NO<sub>y</sub>, H<sub>2</sub>O<sub>2</sub> and HNO<sub>3</sub> as indicators for ozone-NO<sub>x</sub>-hydrocarbon sensitivity in urban  
843 locations, J. Geophys. Res., 100, 14175–14188, 1995.

844 Sinha, V., Kumar, V., and Sarkar, C.: Chemical composition of pre-monsoon air in the Indo-Gangetic Plain  
845 measured using a new PTR-MS and air quality facility: high surface ozone and strong influence of biomass  
846 burning, Atmos. Chem. Phys., 14, 5921-5941, 2014.

847 Stauffer, D. R., and Seaman, N. L.: Use of four-dimensional data assimilation in a limited area mesoscale model.  
848 Part I: Experiments with synoptic-scale data, Monthly Weather Review 118, 1250- 1277, 1990.

849 Stauffer, D. R., Seaman, N. L. and Binkowski, F. S.: Use of four-dimensional data assimilation in a limited-area  
850 mesoscale model. Part II: Effects of data assimilation within the planetary boundary layer, Monthly Weather  
851 Review 119, 734-754, 1991.

852 Stockwell, W. R., Middleton, P., Chang, J. S., and Tang, X.: The second generation regional Acid Deposition  
853 Model chemical mechanism for regional air quality modeling, J. Geophys. Res., 95, 16343-16367, 1990.

854 Taylor, K. E.: Summarizing multiple aspects of model performance in a single diagram, J. Geophys. Res. 106:  
855 7183–7192, 2001.

856 Tewari, M., Chen, F., Wang, W., Dudhia, J., Lemone, M. A., Mitchell, K. E., Ek, M., Gayno, G., Wegiel, J. W.  
857 and Cuenca, R.: Implementation and verification of the unified Noah land-surface model in the WRF model, 20th  
858 Conference on Weather Analysis and Forecasting/16th Conference on Numerical Weather Prediction, Seattle,  
859 WA, American Meteorological Society, 2004.

860 [Tie, X., Geng, F., Guenther, A., Cao, J., Greenberg, J., Zhang, R., Apel, E., Li, G., Weinheimer, A., Chen, J., and](#)  
861 [Cai, C.: Megacity impacts on regional ozone formation: observations and WRF-Chem modeling for the MIRA GE-](#)  
862 [Shanghai field campaign, Atmos. Chem. Phys., 13, 5655-5669, <https://doi.org/10.5194/acp-13-5655-2013>, 2013.](#)

863 Wiedinmyer, C., Akagi, S. K., Yokelson, R. J., Emmons, L. K., Al-Saadi, J. A., Orlando, J. J., and Soja, A. J.: The  
864 Fire INventory from NCAR (FINN): a high resolution global model to estimate the emissions from open burning,  
865 Geosci. Model Dev., 4, 625–641, doi:10.5194/gmd-4-625-2011, 2011.

- Wild, O., Zhu, X. and Prather, M. J.: Fast-J: Accurate simulation of in- and below cloud photolysis in tropospheric chemical models, *Journal of Atmospheric Chemistry*, 37, 245-282, 2000.
- Wilkinson, S., Mills, G., Illidge, R., and Davies, W. J.: How is ozone pollution reducing our food supply?, *J. Exp. Bot.*, 63, 527–536, doi:10.1093/jxb/err317, 2012.
- Yadav, R., Sahu, L. K., Jaaffrey, S. N. A., and Beig, G.: Distributions of ozone and related trace gases at an urban site in western India. *J. Atmos. Chem.* 71, 125–144, 2014.
- Yang, M., Howell, S. G., Zhuang, J., and Huebert, B. J.: Attribution of aerosol light absorption to black carbon, brown carbon, and dust in China – interpretations of atmospheric measurements during EAST-AIRE, *Atmos. Chem. Phys.*, 9, 2035–2050, doi:10.5194/acp-9-2035-2009, 2009.
- Yoon, J. and Pozzer, A.: Model-simulated trend of surface carbon monoxide for the 2001–2010 decade, *Atmos. Chem. Phys.*, 14, 10465-10482, doi:10.5194/acp-14-10465-2014, 2014.
- Zanis, P., Hadjinicolaou, P., Pozzer, A., Tyrllis, E., Dafka, S., Mihalopoulos, N., and Lelieveld, J.: Summertime free-tropospheric ozone pool over the eastern Mediterranean/Middle East, *Atmos. Chem. Phys.*, 14, 115-132, doi:10.5194/acp-14-115-2014, 2014.
- Zaveri, R. A. and Peters, L. K.: A new lumped structure photochemical mechanism for large-scale applications, JOURNAL OF GEOPHYSICAL RESEARCH, VOL. 104, NO. D23, PAGES 30387-30415, 1999.
- Zhang, Q., Streets, D. G., Carmichael, G. R., He, K. B., Huo, H., Kannari, A., Klimont, Z., Park, I. S., Reddy, S., Fu, J. S., Chen, D., Duan, L., Lei, Y., Wang, L. T., and Yao, Z. L.: Asian emissions in 2006 for the NASA INTEX-B mission, *Atmos. Chem. Phys.*, 9, 5131–5153, doi:10.5194/acp-9-5131-2009, 2009.

896 **Table 1.** Abbreviations/ Acronym

EDGAR	Emission Database for Global Atmospheric Research
HTAP	Hemispheric Transport of Air Pollution
IGP	Indo Gangetic plain
IST	Indian standard time
INTEX-B	Intercontinental Chemical Transport Experiment Phase B
MB	Mean Bias
MOZART	Model for Ozone and Related Chemical Tracers
NMB	Normalized mean bias
PBL	Planetary boundary layer
RMSD	Centered root mean squared difference
RRTM	Rapid Radiative Transfer Model
SEAC4RS	Southeast Asia Composition, Cloud, Climate Coupling Regional Study
WRF-Chem	Weather research and forecasting model coupled with chemistry

897

898

899 **Table 2.** Sub-regional estimates of anthropogenic emissions (in million mol h<sup>-1</sup>) in the three emission inventories  
900 used.

Region	HTAP			INTEX-B			SEAC4RS		
	NO <sub>x</sub>	NMVOC	CO	NO <sub>x</sub>	NMVOC	CO	NO <sub>x</sub>	NMVOC	CO
North	8.1	14.0	110.0	6.3	10.0	96.1	8.7	10.7	86.9
East	5.8	10.1	102.9	6.0	6.9	78.8	6.7	8.2	72.4
West	2.9	4.6	31.0	1.8	2.1	24.7	3.7	2.9	24.3
Central	4.6	4.2	44.6	2.0	2.9	34.7	4.9	3.1	26.2
South	5.4	5.8	37.2	2.7	4.1	46.2	3.5	3.4	28.3
Total	26.8	38.7	325.7	18.8	26.0	280.5	27.5	28.3	238

901

902

903 **Table 3.** A brief description of the different WRF-Chem simulations conducted.

Sr. No.	Simulation name	Emission Inventory	Year of Emission Inventory	Spatial Resolution of Emission Inventory	Chemical Mechanism
1	HTAP-RADM2	HTAP	2010	0.1°x 0.1°	RADM2
2	INTEX-RADM2	INTEX-B	2006	0.5°x 0.5°	RADM2
3	S4RS-RADM2	SEAC4RS	2012	0.1°x 0.1°	RADM2
4	HTAP-MOZ	HTAP	2010	0.1°x 0.1°	MOZART-4

904

905

906

907

908

909

910

911

**Table 4.** List of observation sites and data sources used. Site nomenclature in brackets in column 1 is used in figures 1, 5, 6, 9 and 10.

Site	Type	Latitude	Longitude	Altitude (m.a.s.l.)	Data period	Reference
Mohali (MOH)	Urban	30.7°N	76.7°N	310	May 2012	Sinha et al. (2014)
Nainital (NTL)	Highly complex	29.37°N	79.45°E	1958	Apr 2011	Sarangi et. al. (2014)
Pantnagar (PNT)	Urban/complex	29.0°N	79.5°E	231	Apr 2009-11	Ojha et al. (2012)
Delhi (DEL)	Urban	28.65°N	77.27°E	220	Apr 2013	SAFAR data
Dibrugarh (DBG)	Rural/complex	27.4°N	94.9°E	111	Apr 2010-13	Bhuyan et al. (2014)
<del>Darjeeling*</del>	<del>Complex</del>	<del>27.01°N</del>	<del>88.25°E</del>	<del>2134</del>	<del>Apr 2004</del>	<del>Lal (2007)</del>
Kanpur (KNP)	Urban	26.46°N	80.33°E	125	Mar-May 2010-13	Gaur et al. (2014)
<del>Mt. Abu (ABU)</del>	<del>Highly complex</del>	<del>24.6°N</del>	<del>72.7°E</del>	<del>1680</del>	<del>Apr 1993-2000</del>	<del>Naja et al. (2003)</del>
Udaipur (UDP)	Urban	24.58°N	73.68°E	598	Apr 2010	Yadav et al. (2014)
Jabalpur (JBL)	Complex	23.17°N	79.92°E	411	Apr 2013	Sarkar et al. (2015)
Ahmedabad (ABD)	Urban	23.03°N	72.58°E	53	May 2011	Mallik et al. (2015)
<del>Haldia (HAL)</del>	<del>Urban/coastal</del>	<del>22.05°N</del>	<del>88.03°E</del>	<del>8</del>	<del>Apr 2004</del>	<del>Purkait et al. (2009)</del>
Bhubaneswar (BBR)	Urban	21.25°N	85.25°E	45	Mar-May 2010	Mahapatra et al. (2012)
<del>Joharapur (JHP)</del>	<del>Rural</del>	<del>19.3°N</del>	<del>75.2°E</del>	<del>474</del>	<del>Apr 2002-2004</del>	<del>Debaje et al. (2006)</del>
Pune (PUN)	Urban	18.54°N	73.81°E	559	Mar-May 2013	SAFAR data; Beig et al. (2007)
Anantapur (ANP)	Rural	14.62°N	77.65°E	331	Apr 2009	Reddy et al. (2010)
Gadanki (GDK)	Rural	13.48°N	79.18°E	375	Mar-May 2010-11	Renuka et al. (2014)
Kannur (KNR)	Rural/coastal	11.9°N	75.4°E	5	Apr 2010	Nishanth et al. (2012)
Thumba/Trivendrum (TRI)	Urban/coastal	8.55°N	77°E	3	Apr 2009	David et al. (2011)

\* At Darjeeling only monthly mean value is available.

**Table 5.** A comparison of correlation coefficients (r) over different regions for the four simulations

Region	HTAP-RADM2	INTEX-RADM2	S4RS-RADM2	HTAP-MOZ
North	0.90	0.86	0.88	0.90
East	0.98	0.97	0.97	0.98
West	0.99	0.98	0.98	0.99
Central	0.70	0.67	0.69	0.75
South	0.99	0.98	0.97	0.97
Overall	0.98	0.97	0.97	0.99

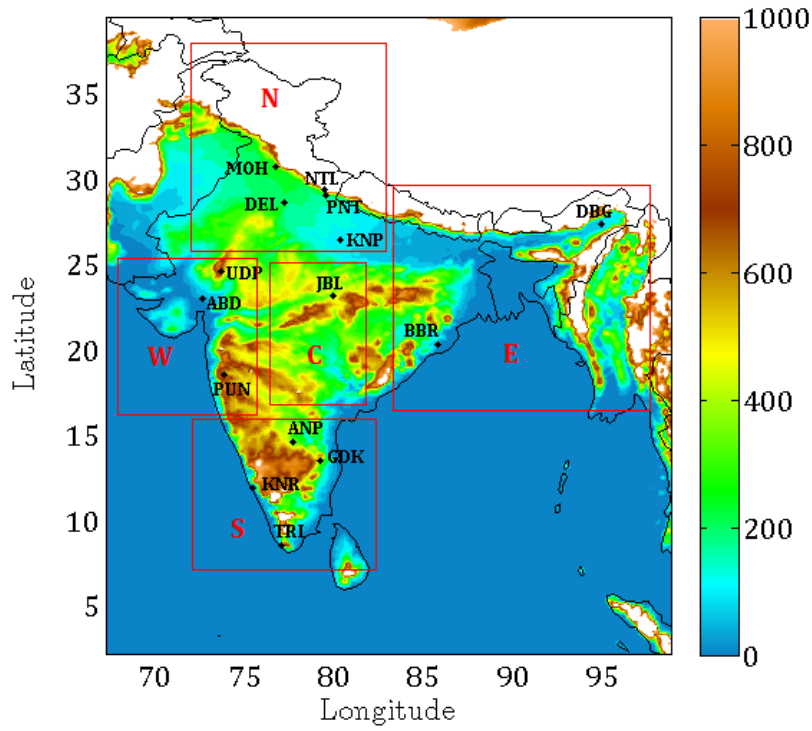


**Table 6.** A comparison of noontime (1130–1630 IST) average mean biases in ppbv over different regions for the four simulations.

Region	HTAP-RADM2	INTEX-RADM2	S4RS-RADM2	HTAP-MOZ
North	2.4	-3.3	-4.1	8.3
East	19.5	21.9	15.9	30.3
West	10.2	7.1	8.1	12.2
Central	0.9	-8.0	-2.5	8.8
South	15.3	8.2	6.5	25.5
Overall	9.6	4.9	3.9	16.6

**Table 7.** Recommendations based on noontime average mean biases over different regions for the four simulations.

Region	HTAP-RADM2	INTEX-RADM2	S4RS-RADM2	HTAP-MOZ
North	✓			
East			✓	
West		✓		
Central	✓			
South			✓	
Overall			✓	



(This figure is revised with old stations removed)

**Figure 1.** Simulation domain showing terrain height (in metres) and observation sites. White region indicates that the terrain height is equal to or exceeds 1 km. The domain is subdivided into five regions viz. North (N), South (S), East (E), West (W) and central (C) regions, as shown by red rectangles.

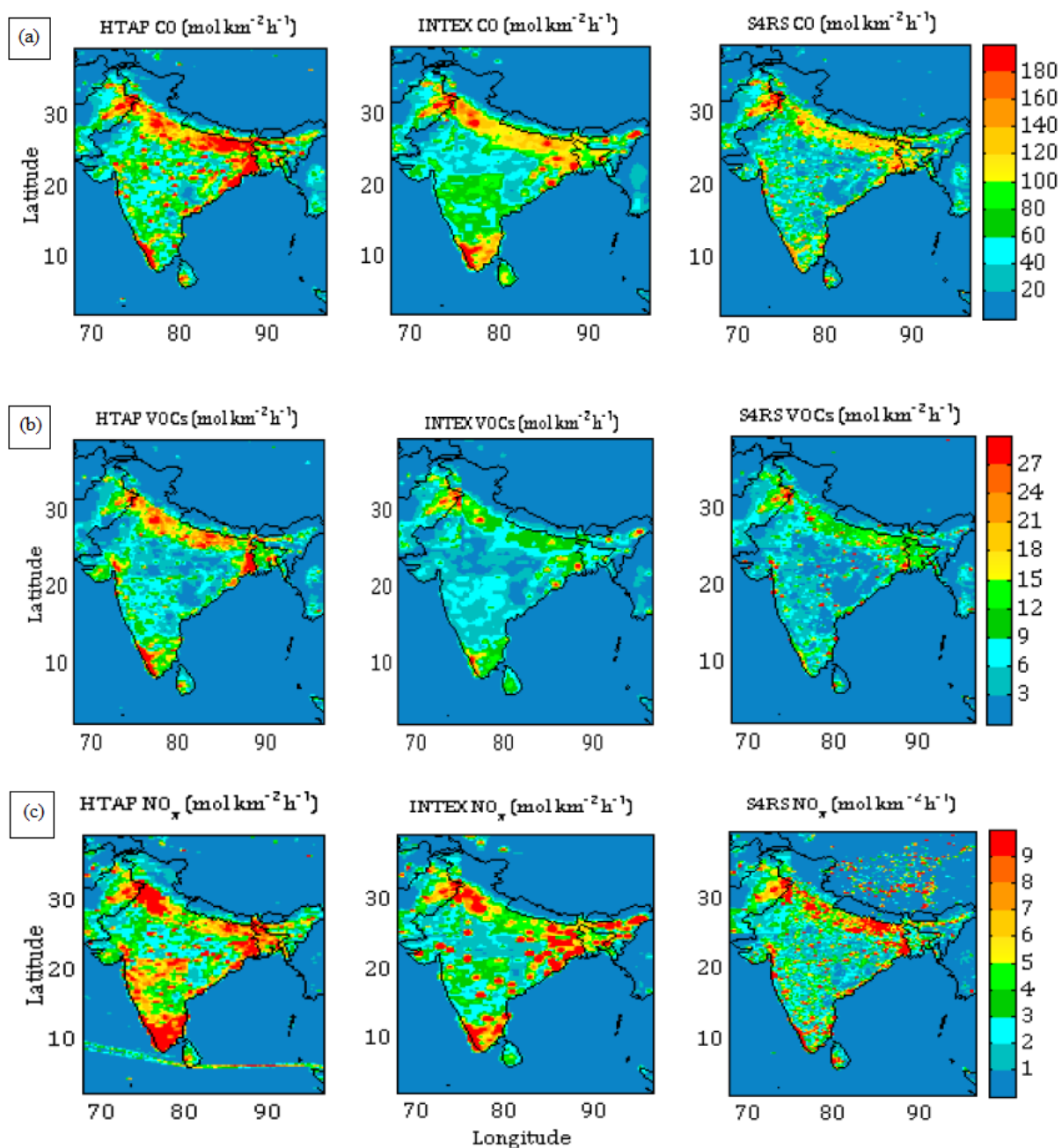
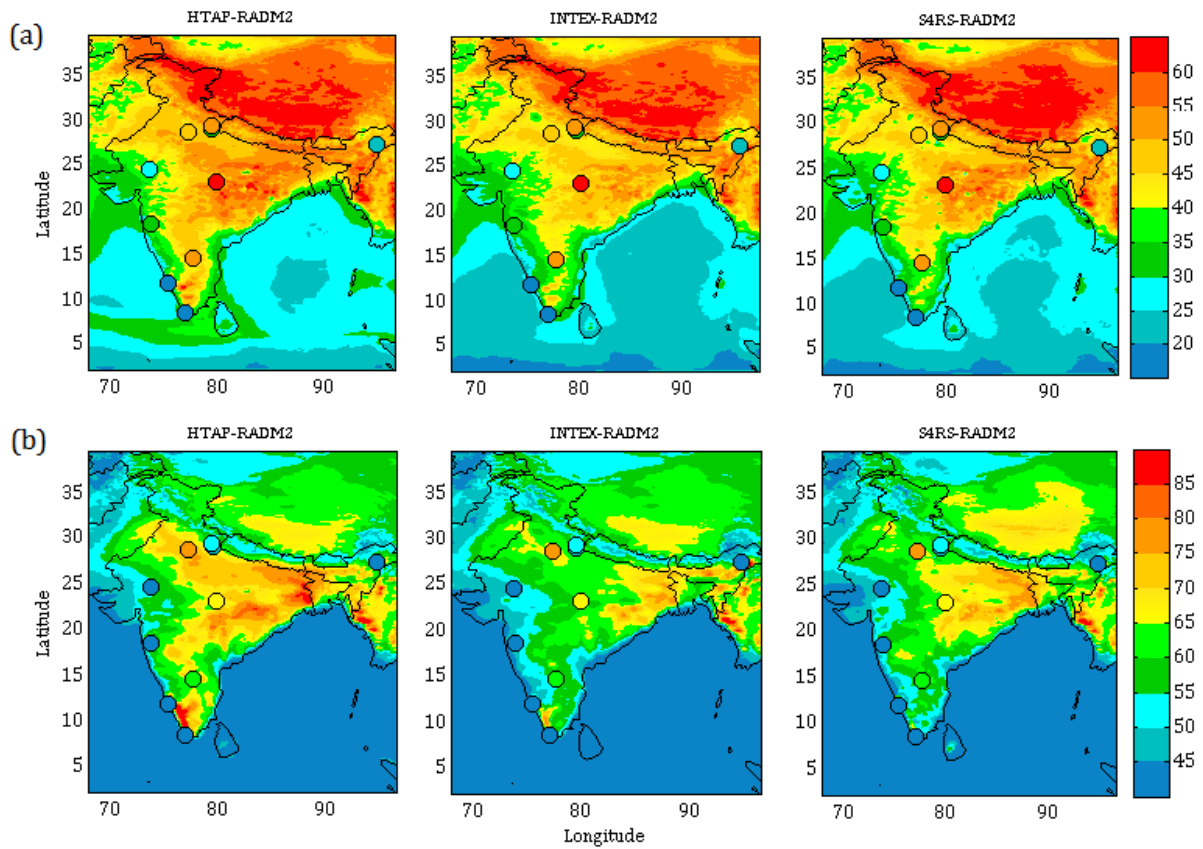


**Figure 2.** Comparison of (a) CO, (b) NM VOC and (c) NO<sub>x</sub> emissions between the three inventories used (see Section-2.2 for description).



(This figure is revised with old stations removed)

**Figure 3.** Monthly (April) average surface ozone calculated for (a) 24 h and (b) noontime (1130-1630 IST). The average ozone mixing ratios (ppbv) from observations are also shown for comparison on the same colour scale. Note the difference in colour scales in the top and bottom rows.

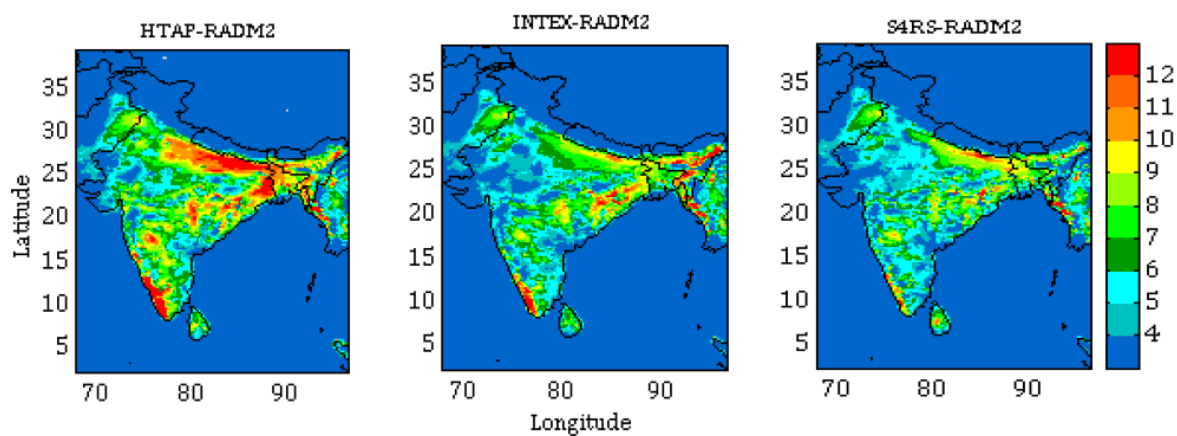


**Figure 4.** Net daytime surface ozone chemical tendency (in ppbv h<sup>-1</sup>) for the month April during 0630-1230 IST.

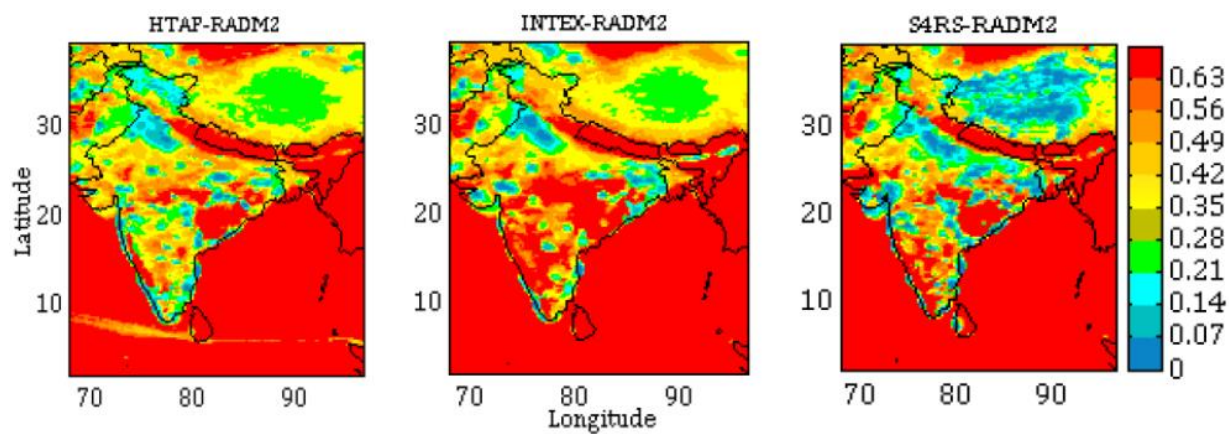
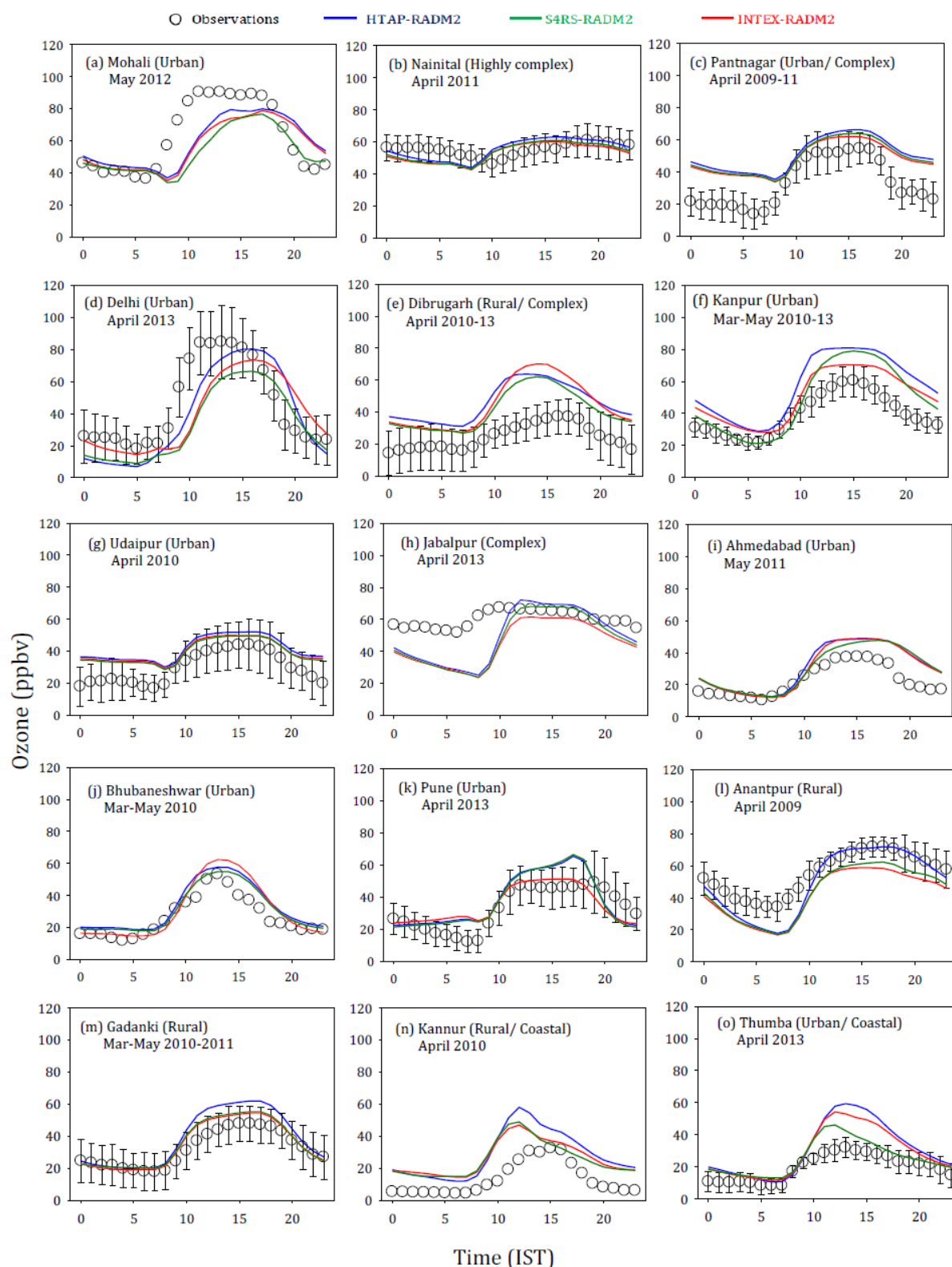


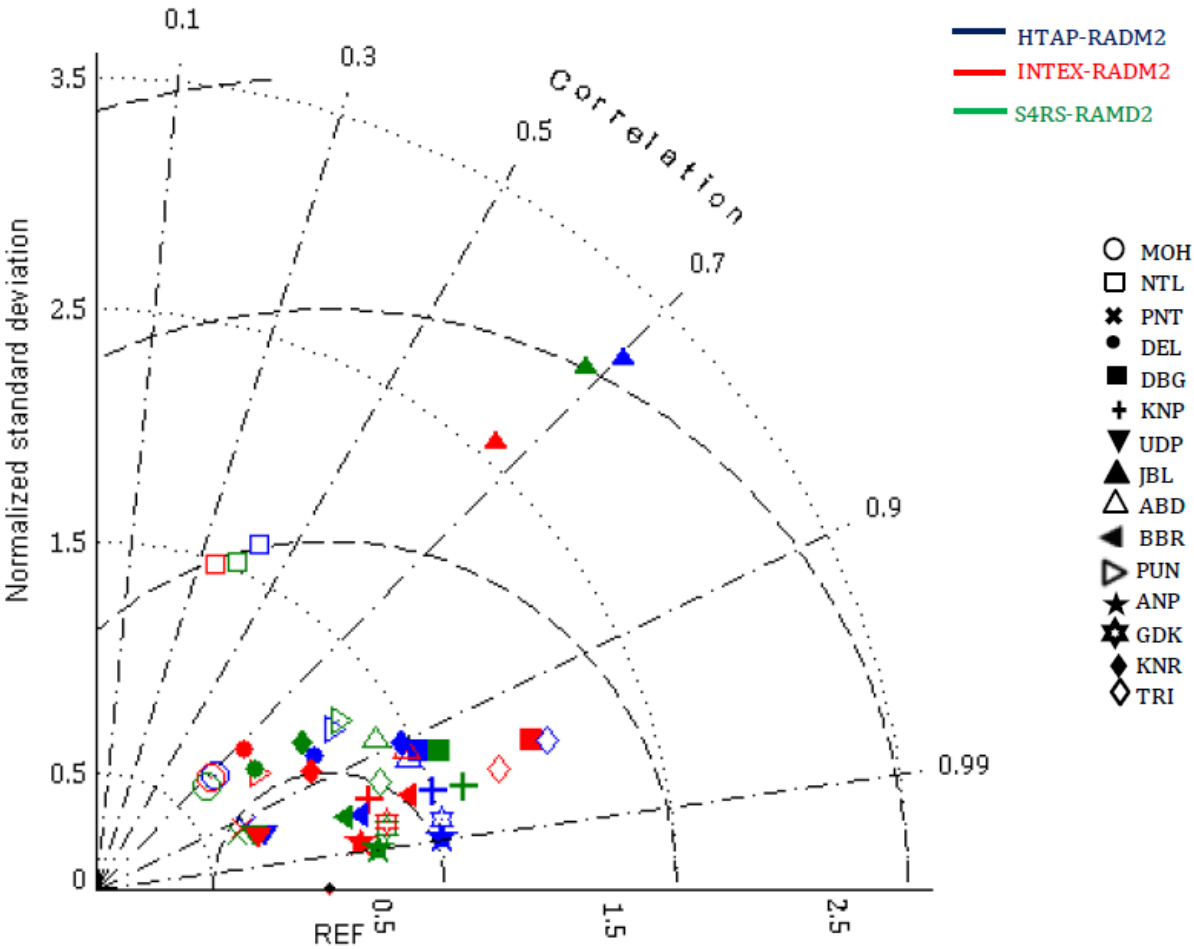
**Figure 5.** Net daytime surface  $\text{CH}_2\text{O}$  to  $\text{NO}_y$  ratio in simulations with different inventories for the month April during 0630-1230 IST.



(This figure is revised with old stations removed)

**Figure 6.** Comparison of monthly average diurnal variation of surface ozone simulated using different emission inventories at various observation sites. The observational data is available for the period indicated in the figure whereas all model simulations are for the year 2013. Error bars represent the temporal standard deviations of the monthly averages. All model simulations are with RADM2 chemistry.

1028



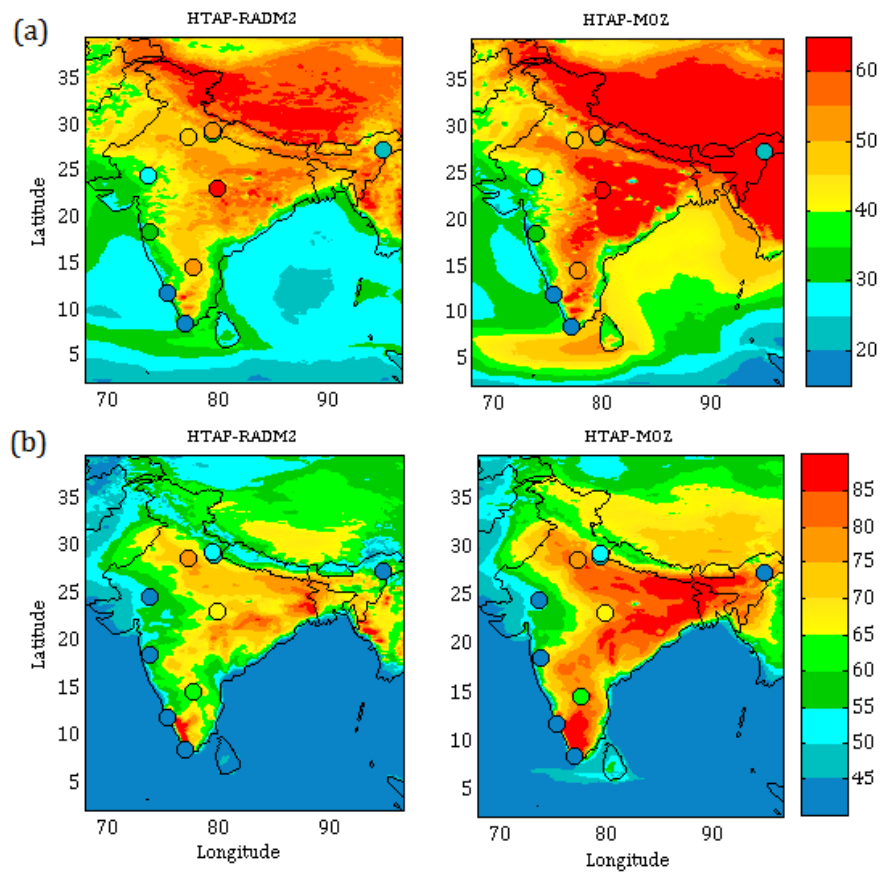
1029  
1030  
1031

(This figure is revised with old stations removed)

1032 **Figure 7.** Taylor diagram with summary model statistics ( $r$ , normalized standard deviation and RMSD) at all sites. The  
1033 correlation is the cosine of the angle from the horizontal axis, the root mean square difference is the distance from the reference  
1034 point (REF) and the standard deviation is the distance from the origin.

1035  
1036  
1037  
1038  
1039  
1040  
1041  
1042





(This figure is revised with old stations removed)

**Figure 8.** Monthly (April) average surface ozone calculated for (a) 24 h and (b) noontime (1130-1630 IST), comparing the chemical mechanisms (RADM2 and MOZART). The average ozone mixing ratios (ppbv) from observations are also shown for comparison on the same colour scale. Note the difference in colour scales in the top and bottom rows.

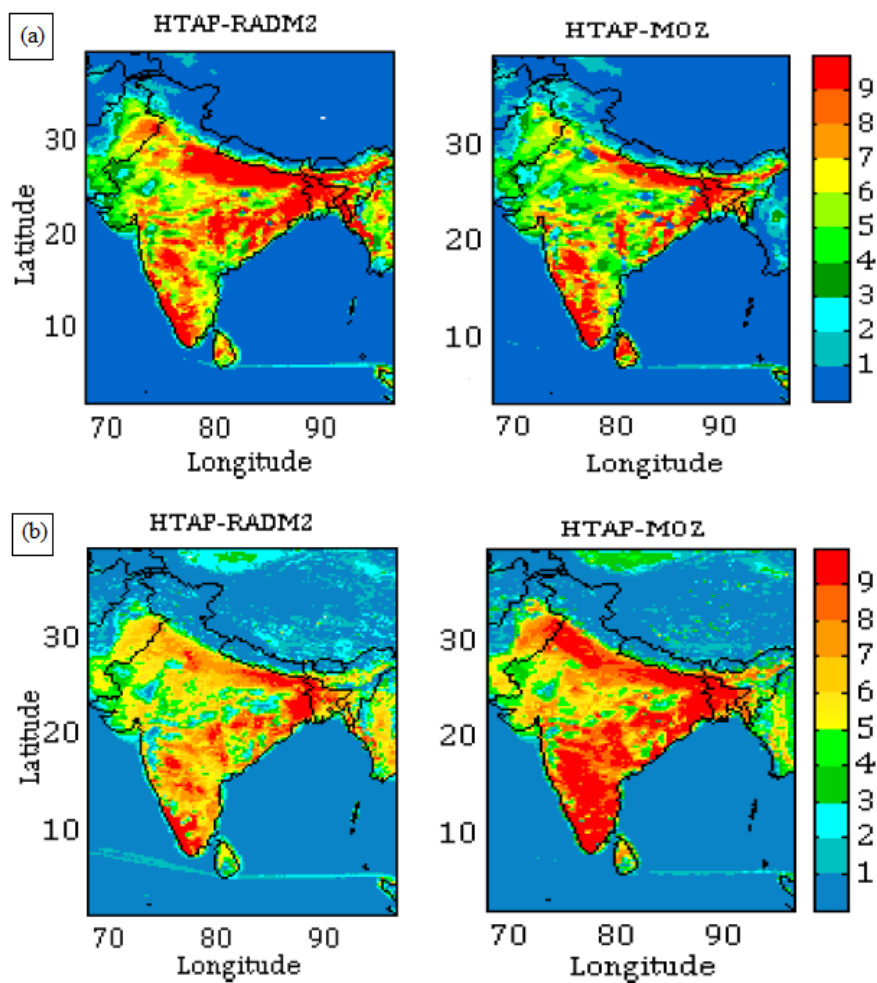


**Figure 9.** Average (a) net daytime surface ozone chemical tendency (in ppbv h<sup>-1</sup>) (b) net daytime surface ozone chemical +vertical mixing tendency (in ppbv h<sup>-1</sup>) for April during 0630-1230 IST

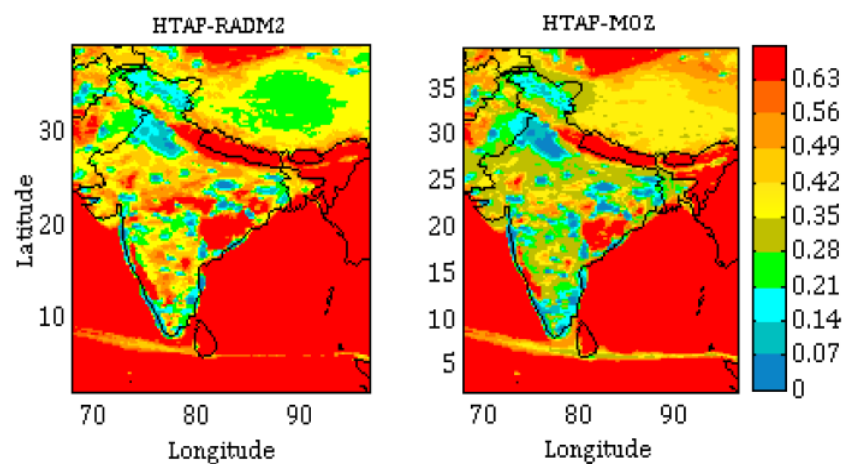
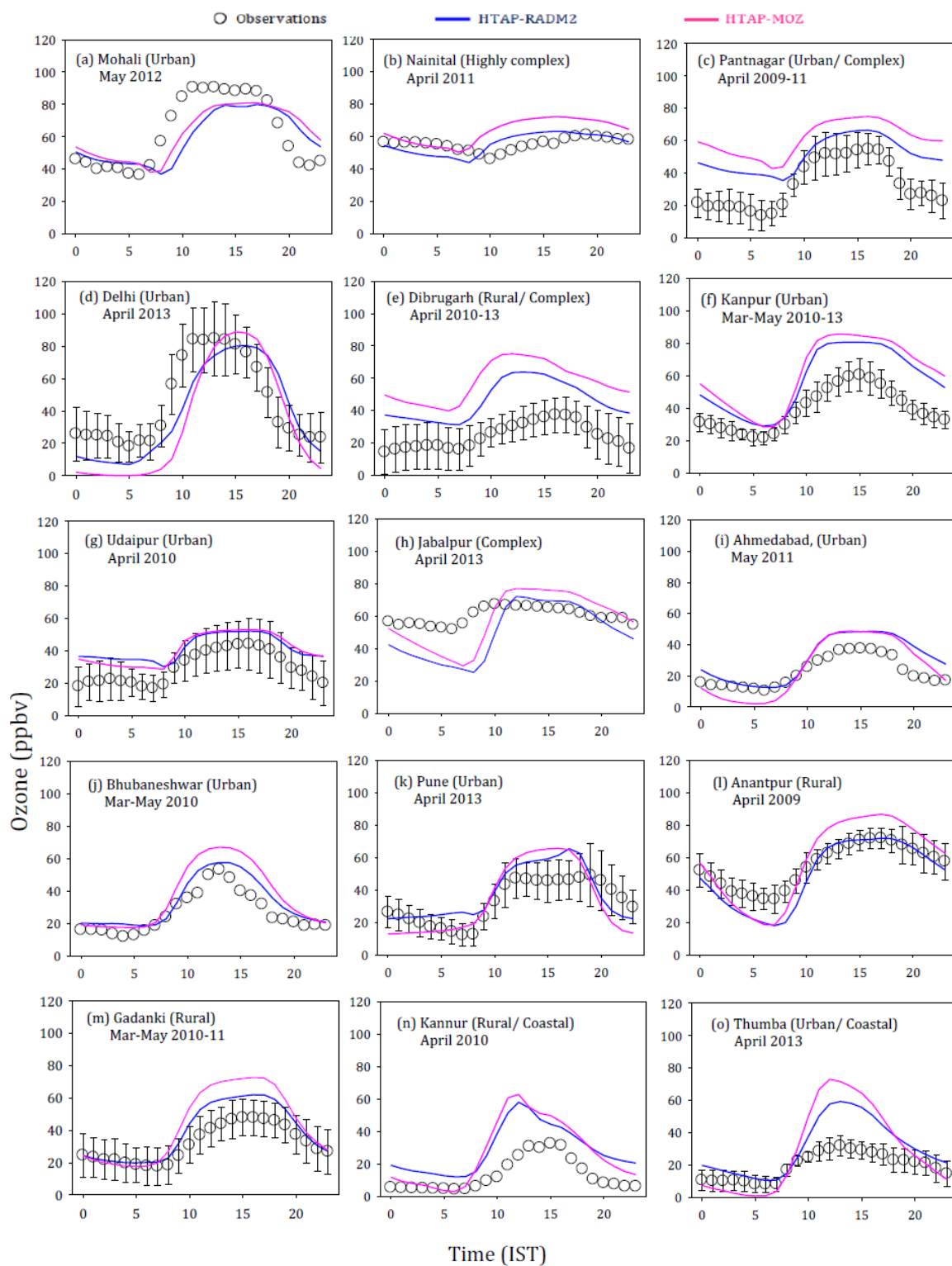
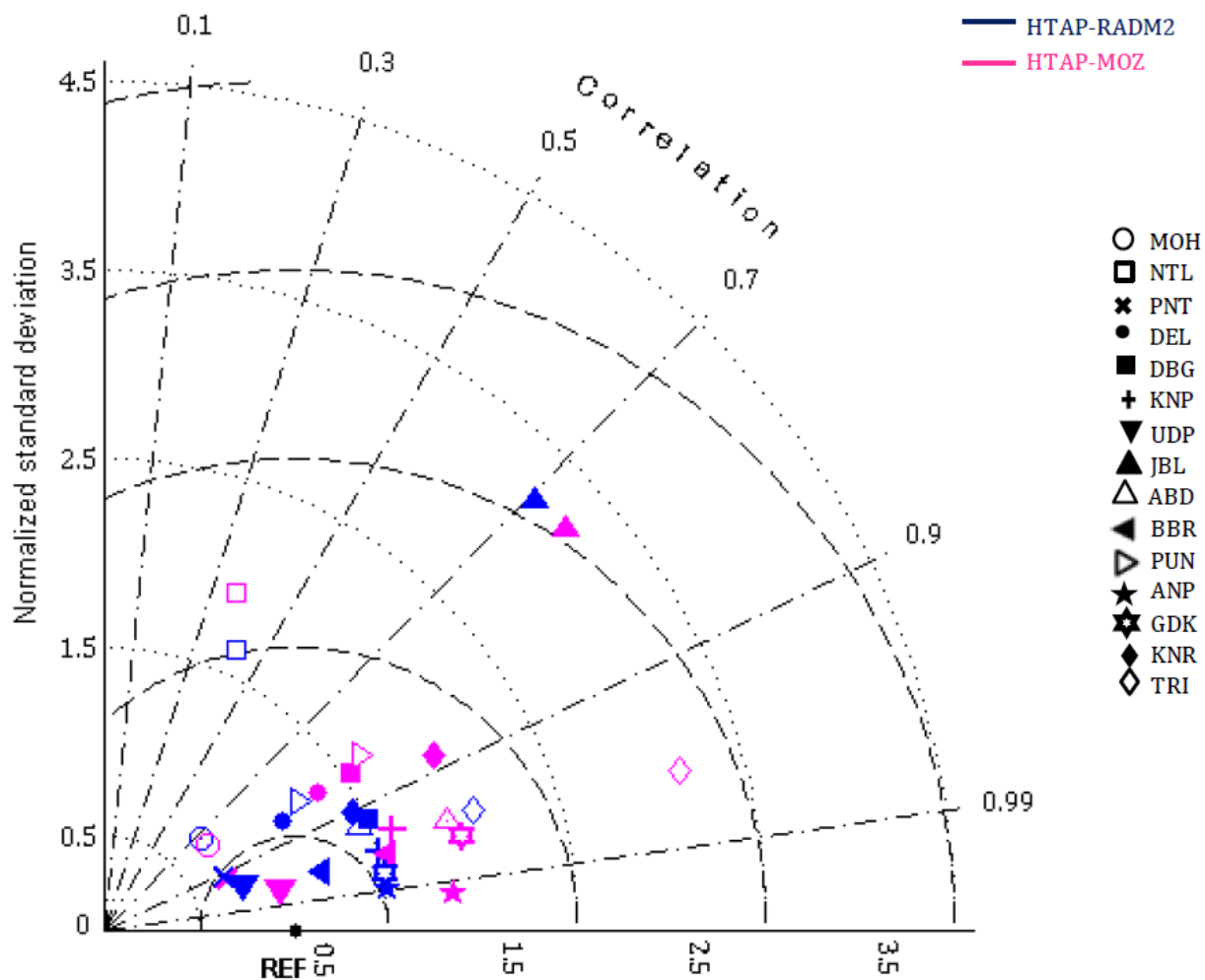


**Figure 10.** Net daytime surface  $\text{CH}_2\text{O}$  to  $\text{NO}_y$  ratio in simulations with different chemical mechanisms for the month April during 0630-1230 IST.



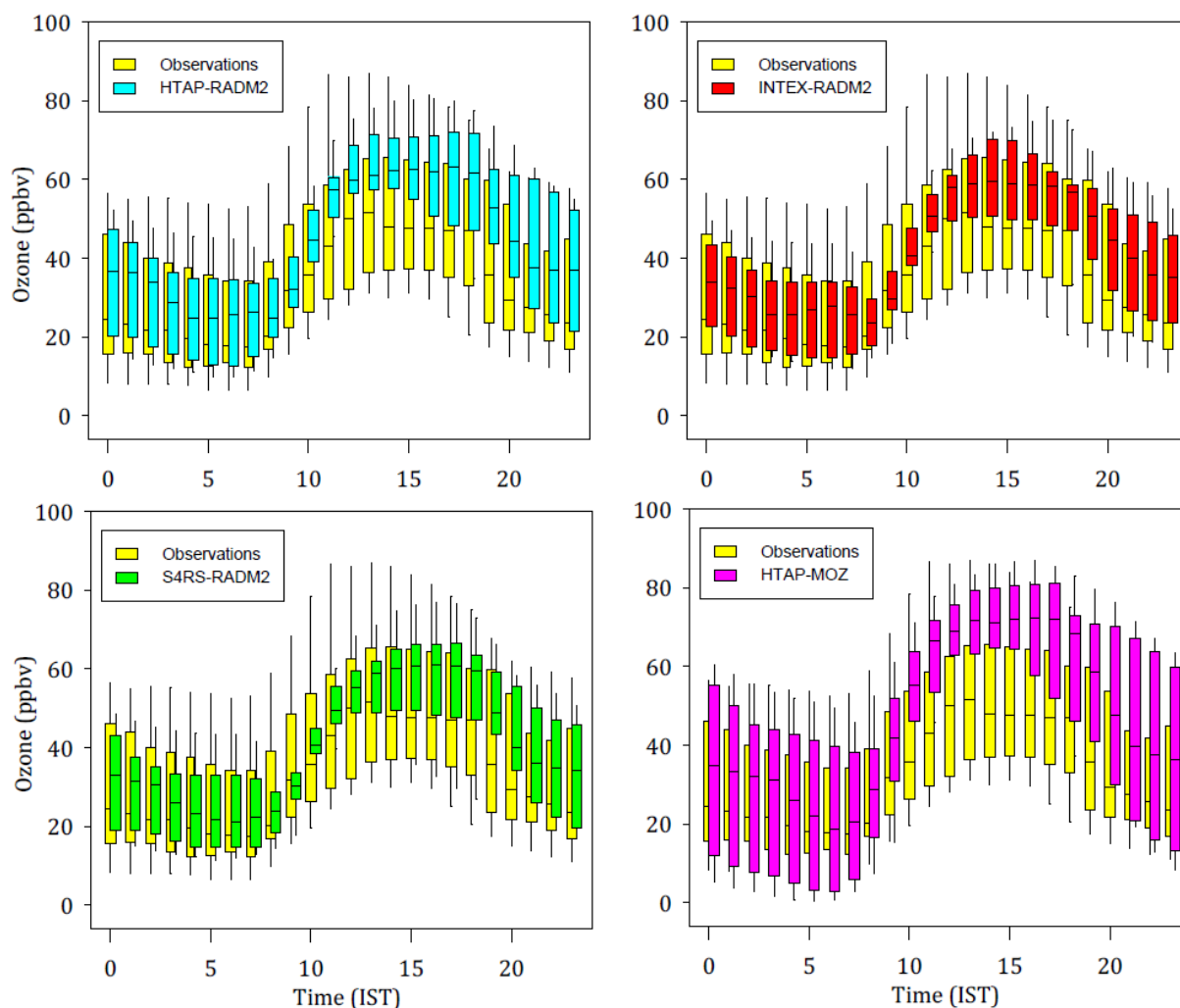
(This figure is revised with old stations removed)

**Figure 11.** Comparison of monthly average diurnal variation of surface ozone simulated using different chemical mechanisms at various observation sites. The observational data is available for the period indicated in the figure whereas all the model simulations are for the year 2013. Error bars represent the temporal standard deviations of the monthly averages. All model simulations are with the HTAP inventory.



(This figure is revised with old stations removed)

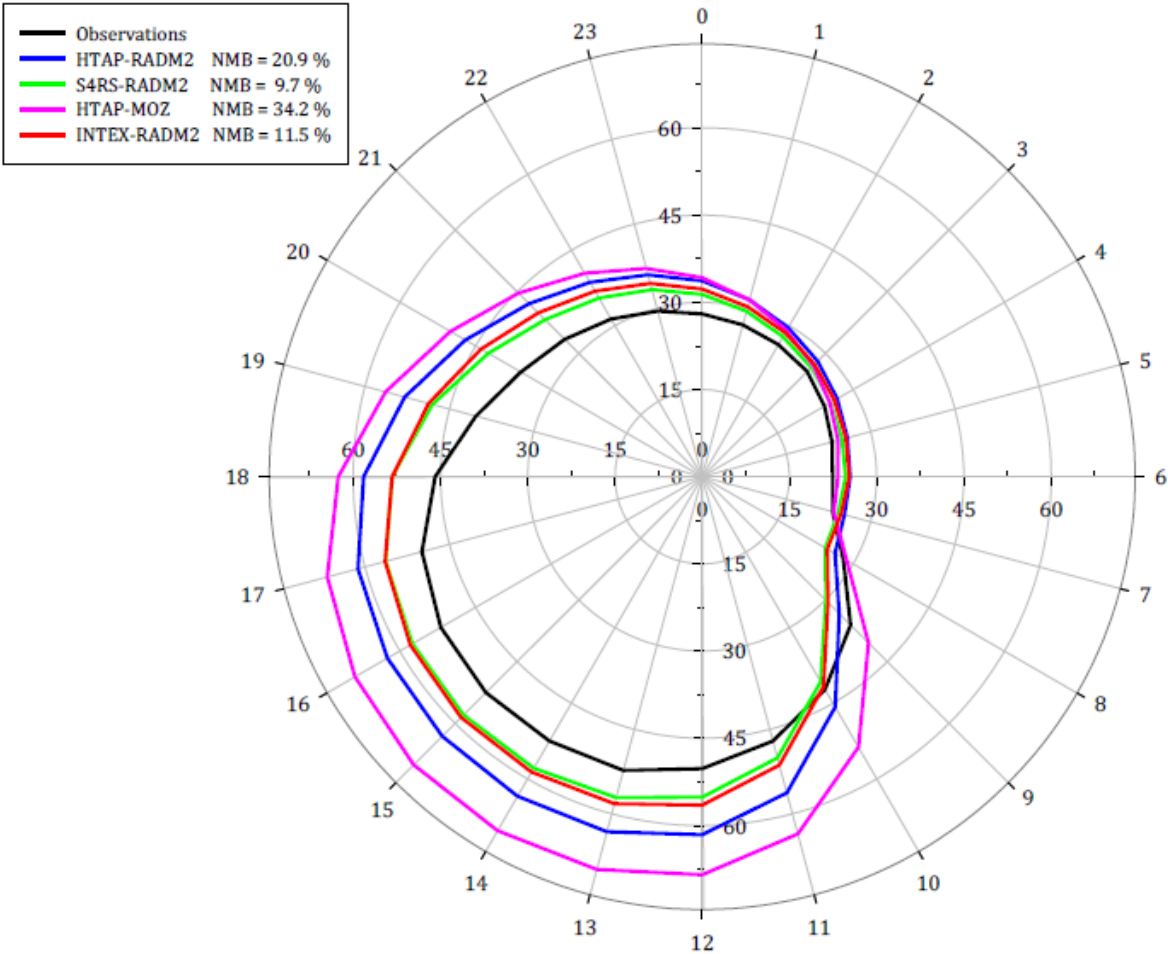
**Figure 12.** Taylor diagram with summary model statistics ( $r$ , normalized standard deviation and RMSD) at all sites. The correlation is the cosine of the angle from the horizontal axis, the root mean square difference is the distance from the reference point (REF) and the standard deviation is the distance from the origin.



(This figure is revised with old stations removed)

**Figure 13.** Box/whisker plot comparison of monthly average diurnal variation of surface ozone from model runs and observations over the entire domain (after spatially averaging the results). Upper and lower boundaries of boxes denote the 75th and 25th percentiles and whiskers represent the 95th and 5th percentiles. The line in the box is the median.

1130



1131

1132

1133

1134

1135

1136

1137

1138

(This figure is revised with old stations removed)

**Figure 14.** Polar plot for monthly mean diurnal variation of surface ozone (in ppbv) from all model simulations and observations each spatially averaged over all sites. The numbers on the outermost circle represent the hour of the day and the radial distance from the centre represents surface ozone mixing ratios in ppbv. The normalized mean biases (NMB in %) for noontime surface ozone are indicated in the caption box.